ELSEVIER

Check for updates

Original Article

Early-age hydration characteristics and kinetics of Portland cement pastes with super low w/c ratios using ice particles as mixing water

Laibo Li[a], Mingxu Chen[a], Xiangyang Guo[b], Lingchao Lu[a,*],
Shoude Wang[a], Xin Cheng[a,*], Kejin Wang[c]

[a] Shandong Provincial Key Lab. of Preparation and Measurement of Building Materials, University of Jinan, Jinan 250022, China
[b] Shandong Provincial Academy of Building Research, Jinan 250000, China
[c] Department of Civil, Construction, and Environmental Engineering, Iowa State University, Ames, IA 50011, United States

ARTICLE INFO

ABSTRACT

The liquid water was replaced by ice particles for preparing homogenous structural Portland cement (PC) pastes at super low w/c ratios from 0.08 to 0.16. For introducing the process of PC hydration, a sophisticated conduction calorimeter was adopted to measure the early-age hydration heat evolution. The hydration kinetic parameters were determined by Krstulovic–Dabic model based on data of hydration heat evolution. The concentrations of K^+ and Na^+ of the pore solution were measured by ICP-OES. Experimental results showed that the acceleration period of the hydration process of PC paste was improved by increasing w/c ratio due to the improvement of space available for hydration product growth. The hydration mechanism of PC paste changed to nucleation and crystal growth (NG) - diffusion (D) when its w/c ratio below 0.16, representing a more intense hydration reaction than that of PC with a normal w/c ratio of 0.30. The concentrations of K^+ and Na^+ of pore solution of hydrated PC paste decreased with the increase of w/c ratios, which led to the alkalinity of that decreased with the increase of w/c ratios. In addition, the mechanical properties of hardened PC pastes were enhanced by increasing w/c ratios from 0.08 to 0.16, which could be attributed to the decrease of porosities of hardened pastes.

1. Introduction

The w/c ratio was one of the key parameters for designing concrete proportioning since it determined the slump of fresh concrete and the capillary porosity, mechanical properties, durability and other engineering properties of hardened concrete [1–3]. The investigation of concrete with low w/c ratios can be dated back to 1970s. Yudenfreund et al. firstly prepared a concrete with compressive strength exceeding 150 MPa at a w/c ratio of 0.2 in 1972 [4]. In the 1980s, Bache [5,6] developed a concrete densified by a high amount of small particles with compressive strength up to 200 MPa, and it has been called DSP concrete. Now, the most widely studied and used low w/c concrete is so-called ultra- high-performance concrete (UHPC). For instance, reactive powder concrete (RPC) is one impor-

tant representation of UHPC. The work of Abid et al. [7–10] indicated that the compressive strength, fracture energy and tensile modulus could respectively exceed 200 MPa, 12 kJ/m^2 and 50 GPa, and the ultimate tensile strain of RPC could reach up to 1.0 %, respectively. Additionally, Cwirzen et al. [6] showed that the surface scaling values of RPC were below 200 g/m^2 and the frost resistance performance of RPC could satisfy the needs of construction with service life for 200 years. Owing to its excellent mechanical and durability properties, UHPC could be used in diverse engineering constructions such as marine, nuclear power and military structures [7,11–15].

The early-age hydration of cement largely determined the setting time and early-age strength of concrete, and the properties as described above were key parameters in the application of concrete [16]. Hence, investigating the early-age hydration characteristics was of interest to scientists and engineers. However, the formation of 'liquid bridges' between cement particles leads to the significant increase of attractive forces between the particles in low w/c systems, which limits the preparation and investigation of that. In general, superplasticizers were adopted to overcome the above problems due to their ability to shield Van-der-Waals force and electrostatic force of powder [17,18]. It is worth noting that a high amount of entrapped air exists in the paste due to the application of superplasticizers, defeating the primary purpose of concrete produced at low w/c ratios. In addition, the complexity of concrete was increased using superplasticizers, which was to the disadvantage of the study of the early-age hydration characteristics and kinetics of cement. Therefore, special methods for preparing the low w/c ratios cement-based materials without any superplasticizer have been explored. For instance, the shear mixing and high-pressure dehydration methods were utilized by Ekincioglu et al. [19] and Živica [3] for producing the cement-based materials with low w/c ratios below 0.1. However, it is easy to form 'liquid bridge' between cement particles due to the physical form of cement and liquid water was different, and the formation of 'liquid bridges' leads to the aggregation of the particles [20,21]. Therefore the removing of micro-bleeding, micro-bulb, settlement and segregation of the concrete with super low w/c ratios is difficult. Hence, the production of the homogenous concrete with super low w/c ratios was still difficult even though the shear mixing method and the high-pressure dehydration technology were utilized.

The physical form of ice particles is solid, which is the same as cement particles. The work of Li et al. [45] on the structure and strength of super low w/c ratios hardened cement paste with indicated that there is only a weak attractive force between ice particles and cement due to the inexistence of 'liquid bridges'. Micro-bleeding, bulb, settlement and segregation could be removed during the mixing of ice particles and cement. Hence, the liquid water was replaced by ice particles for preparing homogenous structural Portland cement (PC) pastes without any superplasticizer at super low w/c ratios. The effects of super low w/c ratios on the early age hydration characteristics, kinetics and other physicochemical properties, such as alkalinity, (i.e., pH), concentrations of K$^+$ and Na$^+$ of pore solution, hydration products, pore structure and mechanical properties were studied. This research could be used in preparing the large-span beams and plates, bridges

Table 1 – Chemical compositions of PCC and slag.

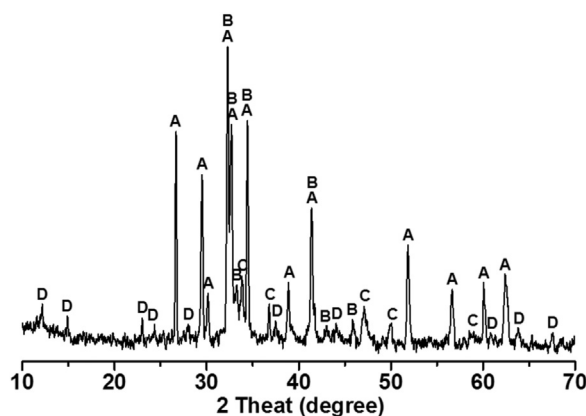| Component	Amount (wt%)	
	PCC	Slag
CaO	64.47	41.74
SiO$_2$	21.79	33.97
Al$_2$O$_3$	4.70	14.53
SO$_3$	0.39	2.12
MgO	4.08	3.34
Fe$_2$O$_3$	3.52	2.28
K$_2$O	0.60	0.30
Na$_2$O	0.20	–
Los	–	1.57

Fig. 1 – X-ray analysis PCC (where A = Tricalcium silicate (C$_3$$), B = Dicalcium silicate (C$_2$$), C = Tricalcium aluminate (C$_3$A), D = Tetracalcium aluminoferrite (C$_4$AF)).

Table 2 – QXRD data of PCC (wt%).

Mineral	C$_3$$	C$_2$$	C$_3$A	C$_4$AF
Content	57.04	22.46	6.37	10.70

and plates of highways and railways and military protection engineering with high-strength et al. Furthermore, this paper aimed to generate useful scientific data for advancing knowledge of high performance concrete made from ice particles at super low w/c ratio.

2. Experimental

2.1. Materials

Portland cement clink (PCC), calcium sulphate dihydrate (CaSO$_4$·2H$_2$O, Purity of ≥99.0 wt %) and slag (Manufactured in Yongfeng science and technology Co., Ltd., China) were mixed and grinded for preparing Portland cement (PC); the mix proportion of PCC, calcium sulphate dihydrate and slag was 75:5:20 by mass. The chemical compositions of PCC and slag were measured by X-ray fluorescence analysis, and are presented in Table 1. X-ray diffraction (XRD) was used to determine the main crystal phases of PCC (Fig. 1 and Table 2). The particle size distribution of PC was determined by the laser particle size analysis (Fig. 2). The physical performance of PC was determined by Chinese National Standard GB 175-2007
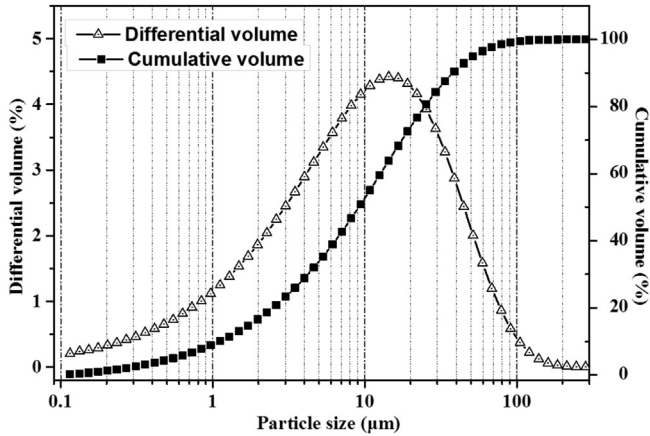
Fig. 2 – Particle size distribution of PC.

Table 3 – Physical properties of PC.	
Properties	Results
Surface area (m^2/kg)	337
Density (kg/m^3)	3050
Unite weight (kg/m^3)	1590
Absolute volume (%)	52.6
Initial setting time (min)	175
Final setting time (min)	232
3-days compressive strength (MPa)	30.5
28-days compressive strength (MPa)	57.2

[22], and the data are shown in Table 3. Additionally, Ca(OH)$_2$, NaOH and KOH were adopted to prepare the solution with pH of 12.4–13.0 for testing the reaction of slag hydration.

Ice particles were used to prepare homogenous structural Portland cement pastes without any superplasticizer. The ice particles were prepared according to [45], and the preparation method was: (1) the supercooled water was atomized in a equipment at $-20 \pm 2\,°C$, and then the liquid water changed into ice particles; (2) the ice particles with sizes above 300 μm were removed by using a square-hole sieve. The preparation of ice particles is presented in Fig. 3. After that, the square-hole sieves with aperture sizes of 90 μm, 98 μm, 105 μm, 125 μm, 154 μm, 200 μm and 300 μm were adopted to test the distribution of ice particles size, and the data are given in Fig. 4.

2.2. Specimens preparation

The cement pastes were prepared by mixing PC and ice particles referring to [45] at w/c ratios of 0.08, 0.10, 0.12, 0.14 and 0.16. After, the cement pastes were sealed in 'Ampoule bottle' for hydration heat measurement. Additionally, the specimens with cavity sizes of $40 \times 40 \times 20\,mm^3$ were produced by pressure molding at a maximum pressure of 25 MPa. The specimens with cavity sizes of $20 \times 20 \times 20\,mm^3$ and $40 \times 20 \times 9\,mm^3$ were accurately cut from the hardened pastes as described. The demoulded specimens were cured in $20 \pm 2\,°C$ and 95+% RH. Furthermore, a normal PC paste was prepared by mixing PC and liquid water at a w/c ratio of 0.30 for comparison to the reference test. The process of specimen preparation and characterizations is presented in Fig. 5.
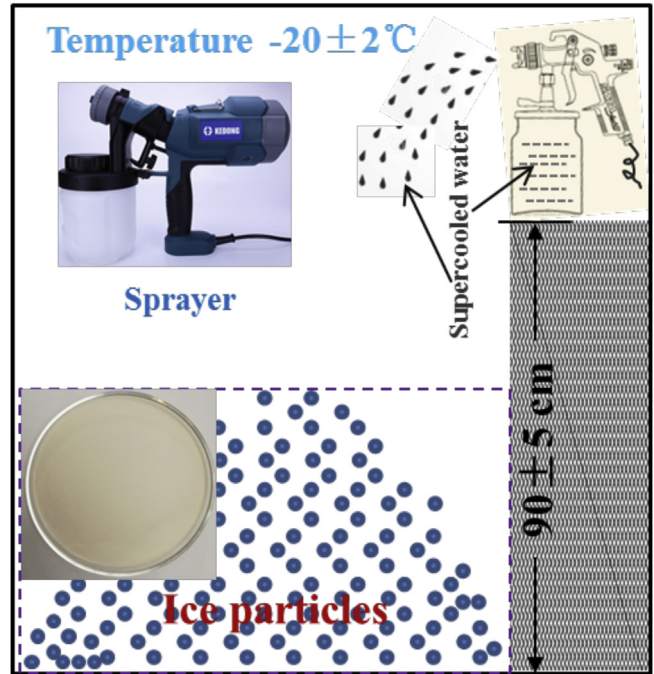

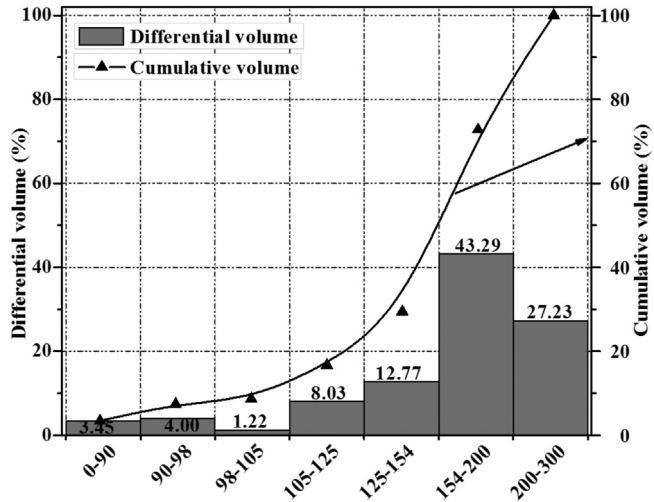Fig. 3 – Set-up of ice particles preparation.

Fig. 4 – Particle size distribution of ice.

2.3. Measurement

2.3.1. Heat of hydration
The hydration heats of PC with different w/c ratio were tested by an accurate conduction calorimeter (TAM Air, USA) in an environment of $20 \pm 2\,°C$. The hydration heat evolutions of slag in solution with different pH values were measured by the same method, and the solutions were prepared with Ca(OH)$_2$, NaOH and KOH.

2.3.2. Hydration kinetics
In the current study, the hydration kinetics were revealed by the Krstulovic–Dabic kinetic model [23,24], which is a classical model for hydration kinetics analysis [23–27]. There are three basic processes during the hydration of cement: nucleation and crystal growth (NG), phase boundary reaction (I),
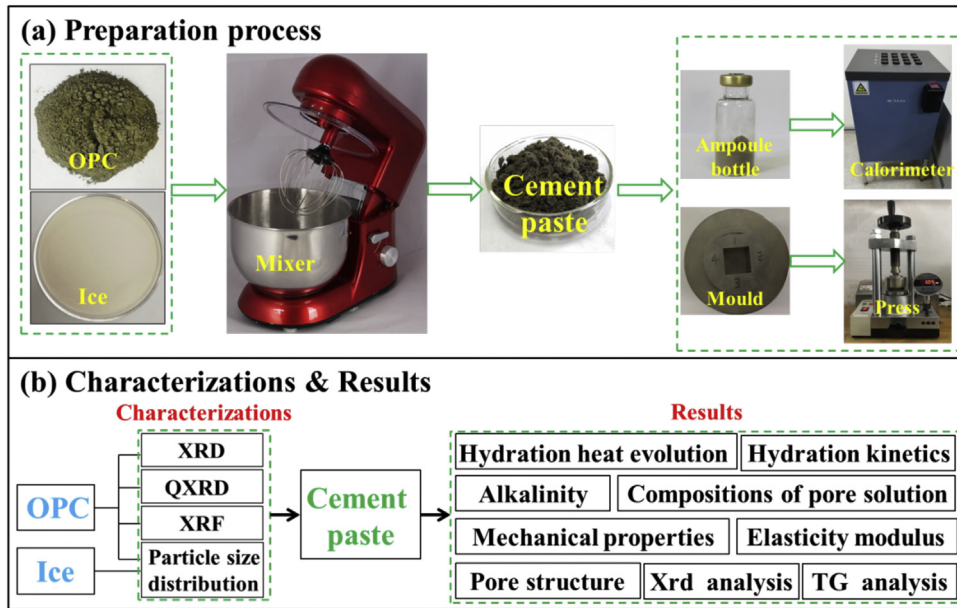
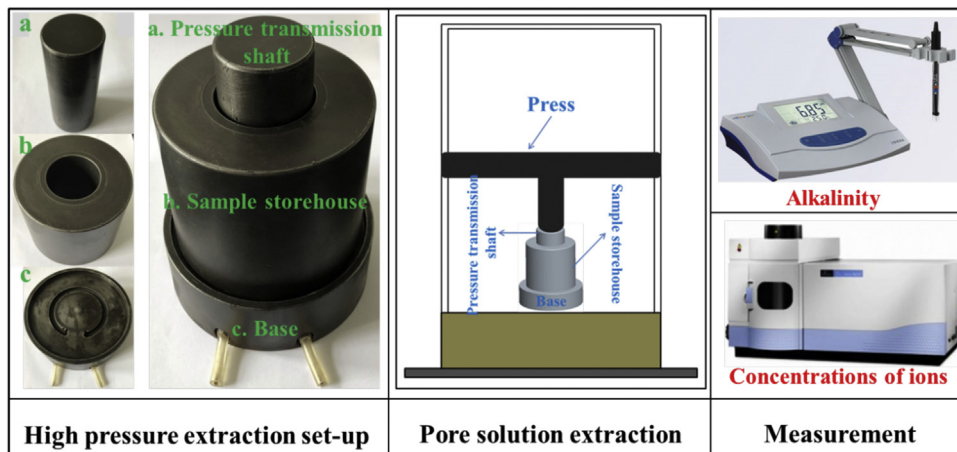Fig. 5 – The flowchart of preparation and characterization of specimens.

Fig. 6 – The high pressure extraction set-up of pore solution of hardened cement pastes.

and diffusion (D) [24]. The processes as described above may occur simultaneously in pairs or alone [24,27]. The hydration mechanism of cement was controlled by the slowest process [23,24]. Furthermore, previous studies [23,28,29] suggested the more detailed about the abovementioned basic processes. The kinetics Eqs. (1), (2), and (3) showed the relationship of the degree and reaction time of hydration for each process.

NG process:

$$[-\ln (1 - \alpha)]^{\frac{1}{n}} = K_1 (t - t_0) = K_1^{'}(t - t_0) \tag{1}$$

I process:

$$[1 - (1 - \alpha)^{\frac{1}{3}}]^1 = K_2 r^{-1} (t - t_0) = K_2^{'}(t - t_0) \tag{2}$$

D process:

$$[1 - (1 - \alpha)^{\frac{1}{3}}]^2 = K_3 r^{-2} (t - t_0) = K_3^{'}(t - t_0) \tag{3}$$

here α is the degree of hydration; n is an geometrical crystal growth exponent; K_1 or $K_1^{'}$, K_2 or $K_2^{'}$ and K_3 or $K_3^{'}$ are constants of hydration rate of NG process, I process and D process; t_0 is the start time of acceleration period; and r is the diameter of the particles involved in hydration reaction.

To describe the hydration rate of NG process, I process and D process, the differential equations can be obtained by differentiating Eqs. (1–3).

NG process:

$$\frac{d\alpha}{dt} = F_1 (\alpha) = K_1^{'} n (1 - \alpha) [-\ln (1 - \alpha)]^{(n-1)/n} \tag{4}$$

I process:

$$\frac{d\alpha}{dt} = F_2 (\alpha) = 3K_2^{'}(1 - \alpha)^{\frac{2}{3}} \tag{5}$$
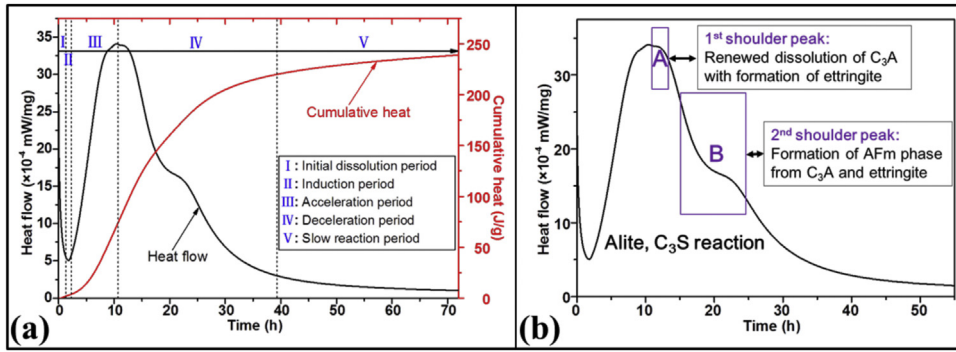
Fig. 7 – (a) Typical heat flow and cumulative heat of early-age hydration of PC with w/c of 0.30; (b) Hydration heat flow of PC with w/c ratio of 0.30, showing typical shoulder peak where a secondary formation of ettringite occurs and subsequent broad peak corresponding to the formation of AFm phase.
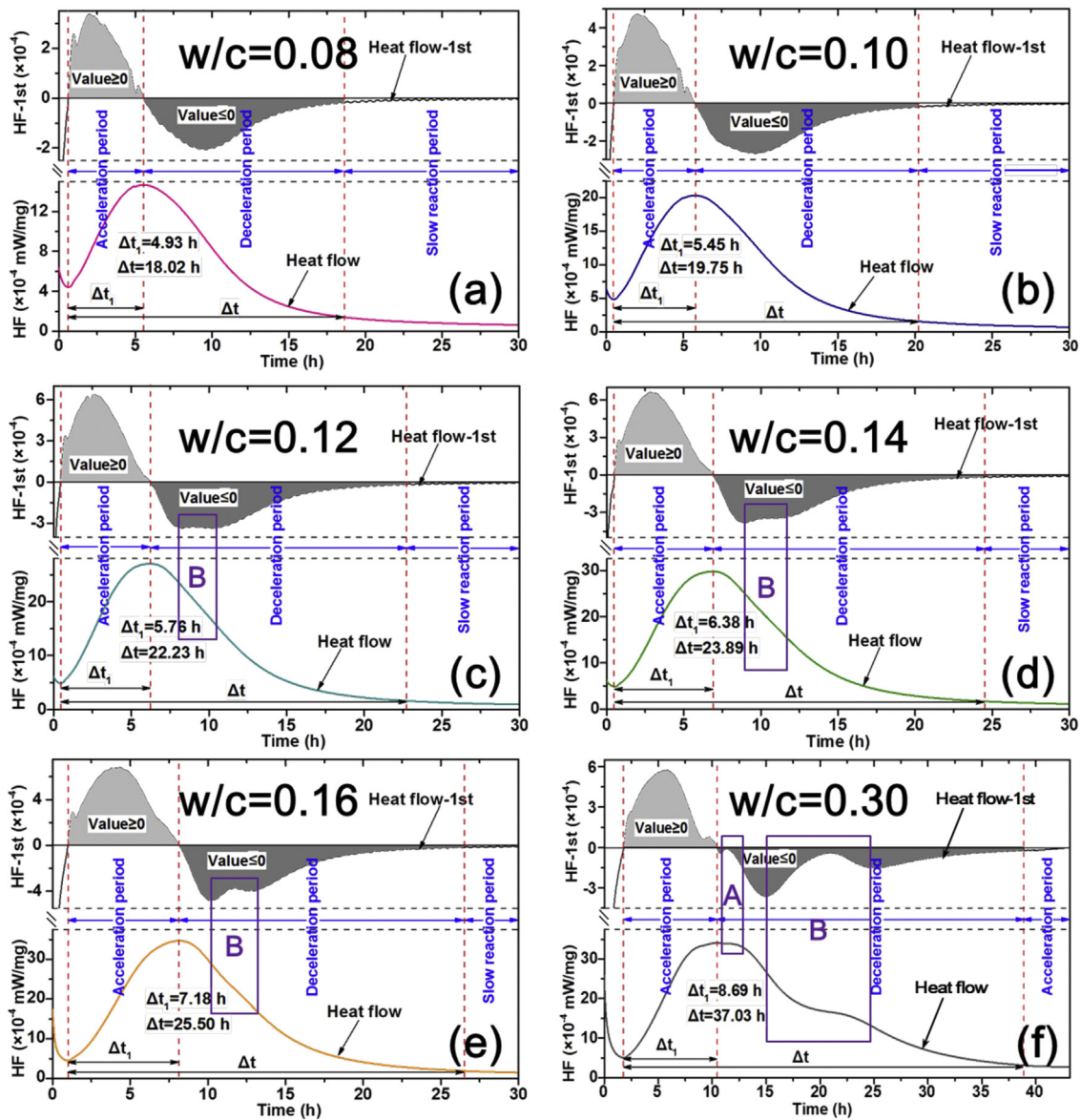

Fig. 8 – Heat flow (HF) and heat flow-1st (HF-1st) of hydration for the Portland cement at different w/c ratios; Δt_1, the time of acceleration period of hydration; Δt, the time of acceleration period and deceleration period of hydration; Area A, the 1st shoulder peak-Corresponding to the secondary formation of ettringite (AFt); Area B, the 2nd shoulder peak-Corresponding to the formation of calcium monosulfoaluminate (AFm).
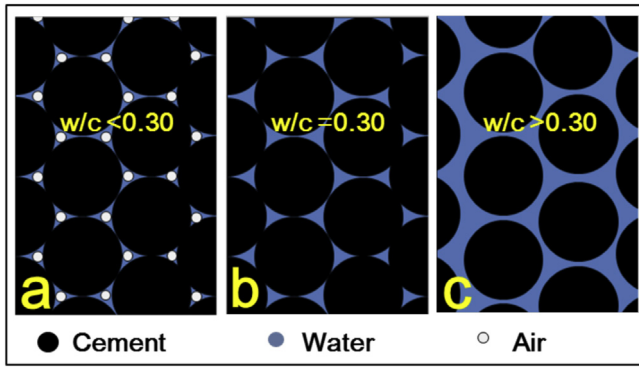
Fig. 9 – Schematic of the distributions of cement particles, water and air in cement pastes. It is clear that if the w/c ratio was less than 0.30, the space could not be totally filled by cement particles and water.

Fig. 10 – Volume distributions of cement particles, water and air of cement pastes with different w/c ratios.

D process:

$$\frac{d\alpha}{dt} = F_3(\alpha) = \frac{3K_3'(1-\alpha)^{2/3}}{2 - 2(1-\alpha)^{1/3}} \qquad (6)$$

where $F_1(\alpha)$, $F_2(\alpha)$ and $F_3(\alpha)$ represent functions of NG, I and D process.

2.3.3. Alkalinity and concentrations of K+ and Na+ of pore solution

The high pressure extraction set-up (Fig. 6) as described in [30] was utilized to extract the pore solution of hydrated paste. A pressure of up to 800 MPa was employed to extract the pore solution from hydrated cement pasts curing for 0.5 h, 1 h, 3 h, 6 h, 12 h, 18 h and 24 h. Then one part of pore solution was diluted by deionized water, and the alkalinity of the solution was tested by an accurate pH meter (PHs-3E, China), whose intrusion accuracy was ±0.01. The other part of pore solution was diluted by nitric acid (0.2 vol%), and the concentrations of K+ and Na+ were tested by using ICP-OES (Optima 5300DV, USA).

2.3.4. Analyses of hydration products

The hydration products were analyzed by thermo-gravimetric (TG) and X-ray diffraction (XRD). TG analysis data were obtained by a TGA/DSC1/1600 H T simultaneous thermal analyzer from 35 °C to 950 °C. In addition, crystallized phases of cement pastes hydrated for 1 day and 3 days were determined by a D8 Advance X-ray diffractometer. The acquisition range of the data was 5–60 degrees (2θ).

2.3.5. Pore structure

Pore structures of 3-days hydrated PC pastes were measured by a Pore Master-60 automatic mercury porosimetry manufactured in USA. The volume of the samples was approximately restricted to 1 cm^3. The pore diameter size was from 5 nm to 200 μm, which depended on the applied pressure.

2.3.6. Mechanical property

The mechanical property of specimens was tested by utilizing a MTS CMT 5504 compression-testing equipment manufactured in USA. The specimens with cavity size of $20 \times 20 \times 20 \text{ mm}^3$ and $40 \times 20 \times 9 \text{ mm}^3$ cured for 1- and 3-days were used to test the compressive strength and flexural strength, respectively.

3. Results and discussion

3.1. Hydration heat evolution

The physical form of ice particles is solid, which was the same as cement. There was only a weak attractive force between ice particles and cement due to the inexistence of 'liquid bridges.' Micro-bleeding, bulb, settlement and segregation could be totally removed and the homogenous structural cement pastes with super low w/c ratios can be prepared by using ice particles as mixing water. Therefore, compared with liquid water, utilizing ice particles can more accurately study the cement hydration process at super low w/c ratios. The overall pattern of hydration of PC was extremely well known.
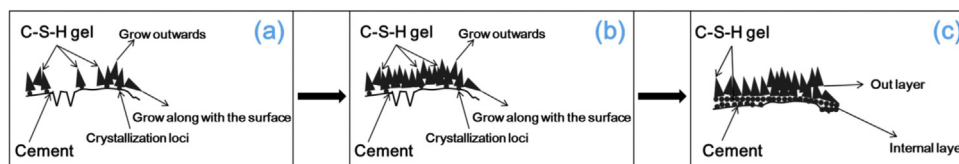

Fig. 11 – Schematic of growth of C-S-H gel in different periods; (a) Growth of C-S-H gel in acceleration period; (b) Growth of C-S-H gel at the division point of acceleration period and deceleration period; (c) Growth of C-S-H gel in deceleration period.
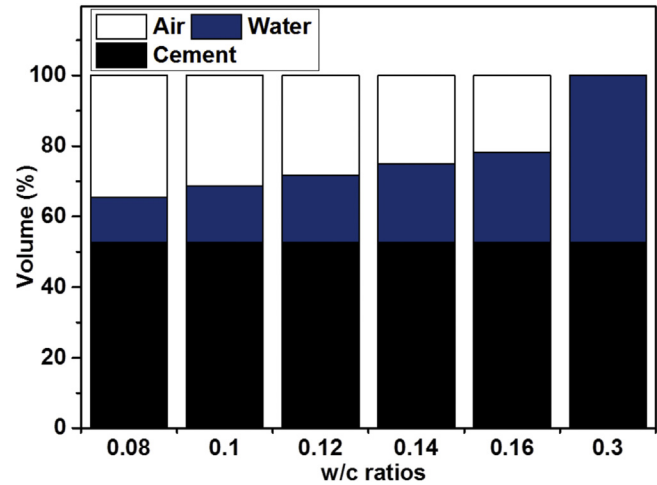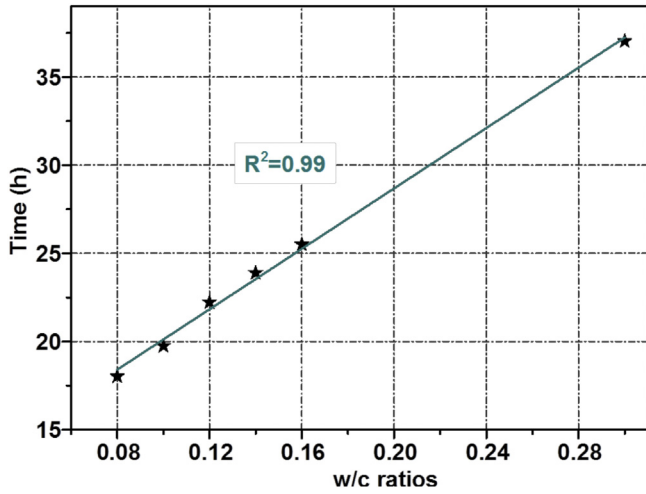
Fig. 12 – Relationship between the time of the main hydration heat peaks (Δt) and w/c ratios.
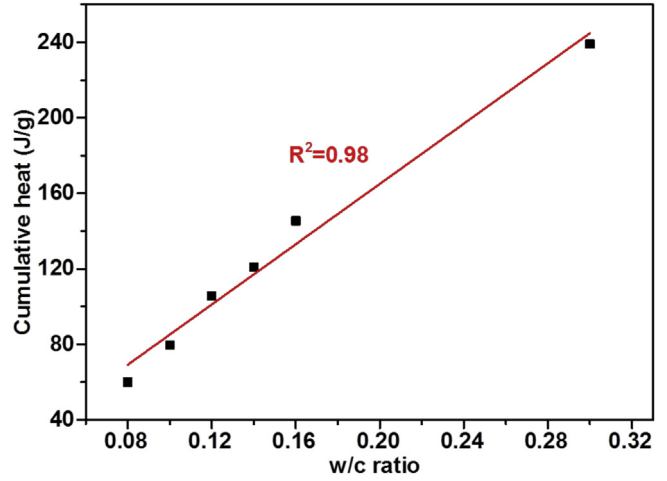

Fig. 14 – Relationship between the 3-days cumulative heat of PC hydration and w/c ratio.
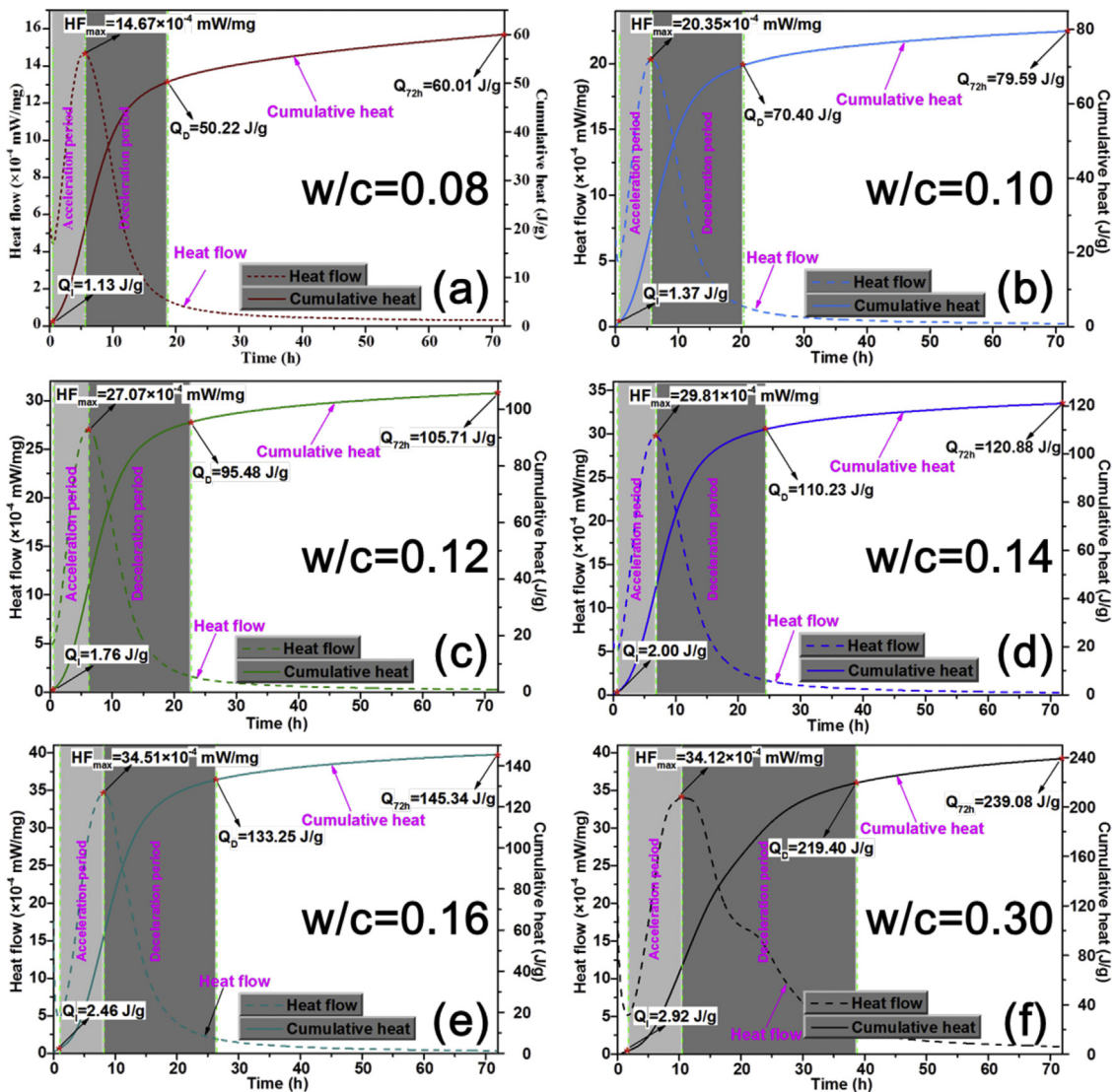

Fig. 13 – Hydration heat evolution of Portland cement.

As shown in Fig. 7(a), the hydration process of PC included generally five periods: (I) initial dissolution period; (II) induction period; (III) acceleration period; (IV) deceleration period; and (V) slow reaction period [31]. However, the current division of the hydration process was somewhat arbitrary due to difficulty in accurate measurement of the division points. In contrast, the division points of the hydration process of PC could be determined by the data from the first differential of heat flow (heat flow-1st), especially for the determination of the acceleration period and deceleration period (Fig. 8). The characteristics of PC hydration at super low w/c ratios mainly included following points:

1   The acceleration period (Δt_1) of PC hydration process was prolonged by raising the w/c ratios. The Δt_1 of sample at w/c of 0.08 was 4.93 h. The Δt_1 of samples with w/c ratios of 0.16 and 0.30 can reach up to 7.18 h and 8.69 h, which were 45.6 % and 76.3 % more than that of the cement paste with a w/c ratio of 0.08. This phenomenon could be ascribed to the space available for C-S-H gel growth increasing with the raising w/c ratios. There were two main views on the end of acceleration period or the occurrence of deceleration period of PC hydration. According to the classical Avrami equation [32], the acceleration period of PC hydration ended when the regions of C-S-H gel growth started to impinge and C-S-H gel covered cement particles totally. In addition, Bazzoni [31,33] suggested that the acceleration period of PC depended on the nucleation and growth of hydration products. The hydration products nucleated and grew on cement particles, and the deceleration occurred when the surface of particles was completely covered by the gel [33]. Therefore, the space available for hydration products growth and the surface of cement available for hydration products precipitation were keys to controlling the acceleration period. The void ratio of cement particle stacking (i.e., the difference of total volume and absolute volume) reached 47.4% (Table 3), which shows that the space could not be filled by cement particles and water unless w/c ratio was more than 0.30, as in Fig. 9. The zone taken up by water was the space available for hydration products growth, and the space increased with increasing w/c ratios (Fig. 10). In a relatively small space, the growth of hydration products was easily impinged, and the hydration products were limited to grow outwards and forced to grow along the surface of cement particles (Fig. 11). In addition, the alkalinity (i.e., pH) of solution depended on the dissolution of Na$^+$ and K$^+$ in early age hydration [34], and the pH of solution probably improved while the w/c ratios decreased. The reaction rate of hydration improved with increasing pH of the solution.

2   The time of main heat evolution peak (Δt, i.e., the time of acceleration period and deceleration period) extended while w/c ratios increased (Fig. 8). Compared with w/c of 0.08, the Δt improved by 105.5 % to a value of 37.03 h when the w/c ratio reached 0.30. Fig. 12 presented an extremely linear correlation of Δt and w/c ratios. However, in comparison studies, there was not much effect on the time of main heat evolution peak in increasing w/c ratios (w/c = 0.4−0.8) [31]. This difference could be attributed to two reasons. First, the space available for C-S-H gel growth increased with increasing w/c ratios as described,

which led to a prolonging of the acceleration period. Second, the mechanism operating in the deceleration period was different from the acceleration period. During the deceleration period, the hydration process was controlled by the osmotic pressure of water between the internal and external outer layer of the C-S-H gel (Fig. 11). The osmotic pressure of water increased with increasing of w/c ratios when the w/c ratios were no more than 0.30. However, when the w/c ratios were more than 0.30, with the w/c ratios increased the osmotic pressure of water was essentially unchanged (Fig. 9). Therefore, the duration of the deceleration period (i.e., the difference between Δt and Δt_1) increased when w/c ratios were less than 0.30.

3   The 1st- and 2nd-shoulder peak could be intuitively found in the PC hydration at w/c of 0.30 (Area A and Area B, Fig. 8 (f)). Bullard et al. [35] suggested that the 1st shoulder peak can be attributed to the C_3A (C = CaO, A = Al$_2$O$_3$) renewed dissolution for forming AFt and the 2nd-shoulder peak can be attributed to the formation of AFm (Fig. 7a). Fig. 8(f) showed the formation of the AFm phase began at 15 h after the experiment started. The study by Minard et al. [36] proved that the gypsum was exhausted at approximately 15–18 h and the hydration of C_3A (i.e., the formation of AFm) began to accelerate. However, the shoulder peak cannot be found in the PC hydration process at w/c ratios below 0.16. The start time of the formation of AFm reduced with a decrease in w/c ratios (Fig. 8c–f). This phenomenon could be explained by that the critical super saturation of AFm became more and more easily when w/c ratios reduced.

4   Fig. 13 showed that the cumulative heat of PC hydration increased with the raising of w/c ratios. For instance, the 3-days cumulative heat of PC hydration at w/c of 0.16 was 145.34 J/g, an improvement of 142.2 % compared with the sample hydrated at w/c of 0.08. Additionally, the relationship the cumulative heats and w/c ratios could be described as a linear correlation (Fig. 14). This phenomenon could be attributed to the amount of PC hydration being mainly determined by w/c and the space available for C-S-H gel growth [31]. In general, the reaction rate increased with the increase of the amount of reactant. Hence, the hydration rate increased with the increase of w/c ratio in theory. This opinion was also supported by Bazzoni [37]. The work of Bazzoni [37] on the early hydration of PC at w/c ratios from 0.3 to 0.8 suggested the maximum value of heat flow (HF$_{max}$, representing the maximum hydration rate) increased significantly with raising w/c even if the value of w/c reached up to 0.80. However, the HF$_{max}$ of w/c of 0.16 was slightly higher more than that of w/c of 0.30 in this particular case (Fig. 13). The possible reason was that the alkalinity of pore solution corresponding to HF$_{max}$ reached up to 13.1 at w/c ratio of 0.16, and the alkalinity corresponding to HF$_{max}$ was only 12.5 at w/c ratio of 0.30 (Fig. 18). The precipitation of CH and the hydration rate of PC were accelerated by increasing alkalinity of pore solution. In addition, the hydration rate of slag in cement increased sharply while the alkalinity of pore solution exceeded 12.6 (Fig. 15).
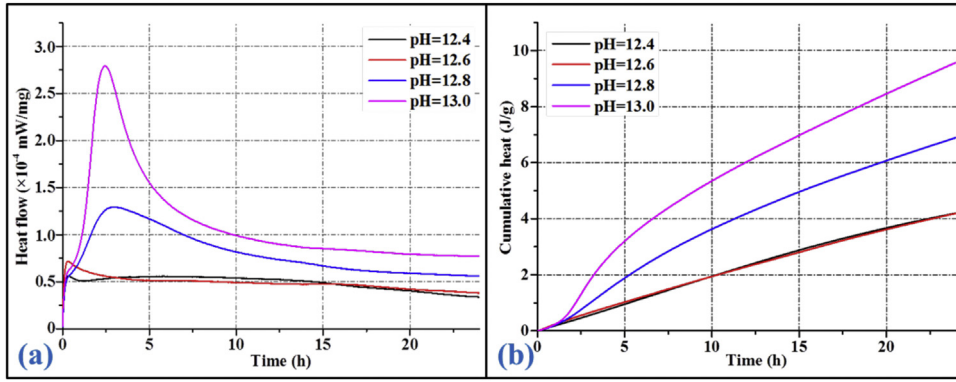
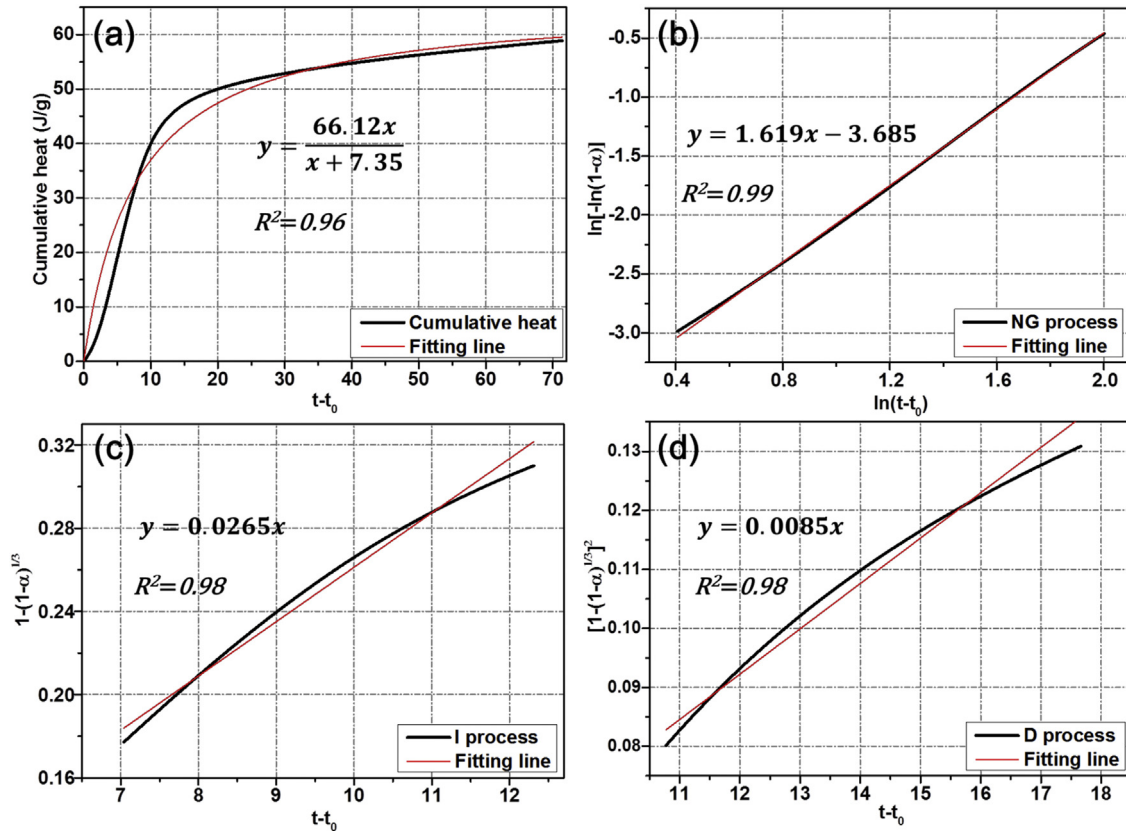Fig. 15 – Reaction of slag in solution with different pH.

Fig. 16 – Calculation of kinetics parameters from the non-linear fitting and linear fitting at w/c ratio of 0.08; (a) Determination of Q_{max} and t_{50}, (b) Determination of n and K_1', (c) Determination of K_2', and (d) Determination of K_3'.

Table 4 – Kinetics parameters of hydration of PC with different w/c ratios.

w/c	n	K_1'	K_2'	K_3'	Hydration mechanism	α_1	α_2	$\Delta\alpha$	t_{50} (h)	Q_{max} (J/g)
0.08	1.619	0.1027	0.0265	0.0085	NG-D	–	0.371	–	7.35	66.12
0.10	1.716	0.1018	0.0260	0.0081	NG-D	–	0.358	–	7.68	89.72
0.12	1.834	0.0994	0.0251	0.0078	NG-D	–	0.352	–	8.11	120.99
0.14	1.886	0.0933	0.0235	0.0072	NG-D	–	0.341	–	8.83	140.38
0.16	1.983	0.0862	0.0216	0.0065	NG-D	–	0.337	–	9.94	170.56
0.30	1.853	0.0526	0.0109	0.0027	NG-I-D	0.188	0.311	0.123	21.44	326.75

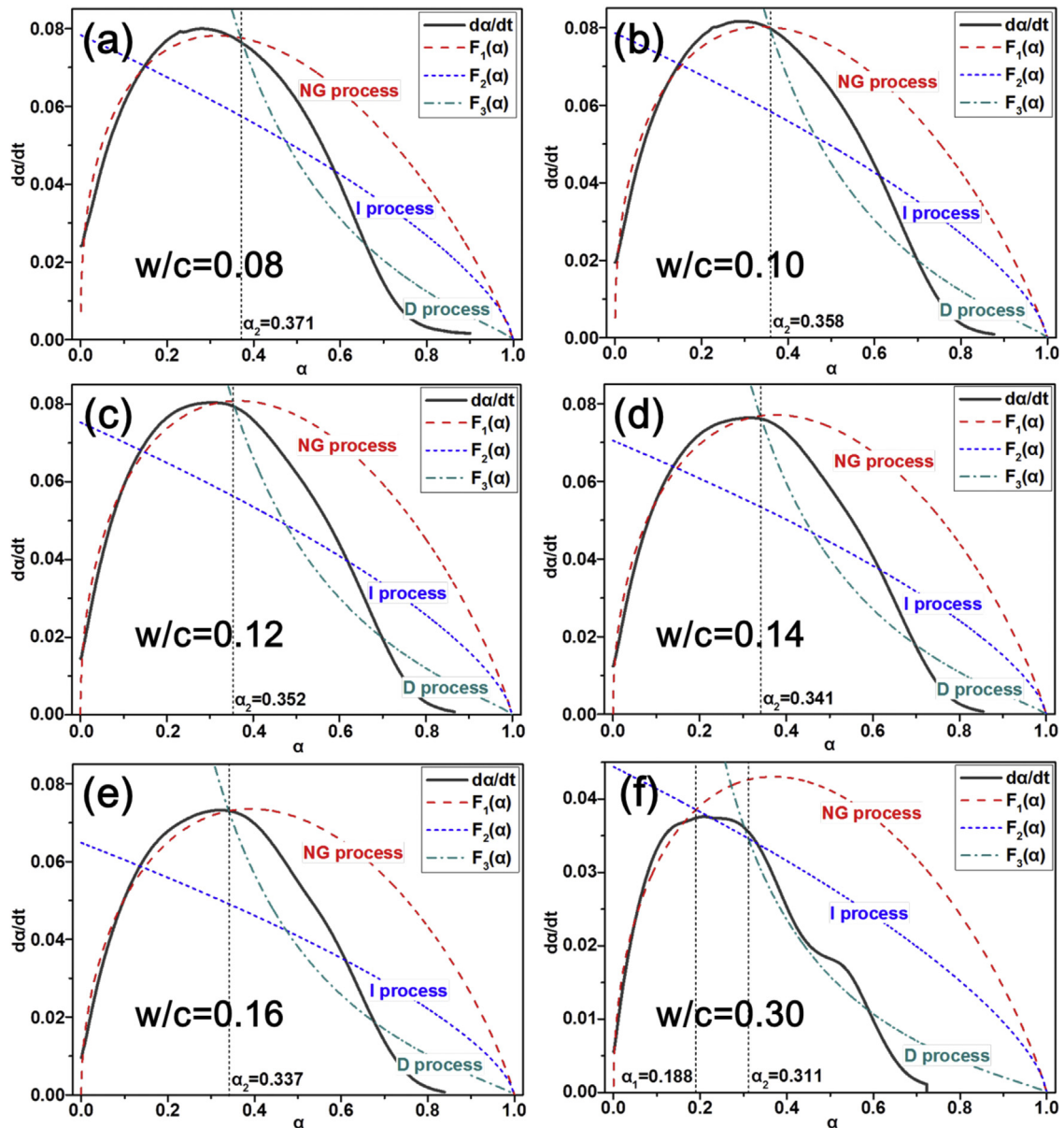$\Delta\alpha$: the difference between α_1 and α_2.

Fig. 17 – Hydration rate curves of PC with different w/c ratios; α_1, the division point of NG process and I process; α_2, the division point of I process and D process.

3.2. Hydration kinetics

3.2.1. Calculation of parameters of hydration kinetics

The quantity of heat released before acceleration period (i.e., in initial hydration period and induction period) can be ignored in the calculation of parameters of hydration kinetics because of it was less than 2 % of total heat (Fig. 13). The degree of hydration (α) could be determined according to Eq. (7), and the dα/dt could be determined by Eq. (8). More importantly, the relationship of $1/Q(t)$ and $1/Q_{max}$, $1/(t-t_0)$ can be established by Kundsen [25,29], as shown in Eq. (9). According to Eq. (9), the relationship between $Q(t)$ and Q_{max}, $t-t_0$ could be determined (i.e., Eq. 10). To determine the Q_{max} and t_{50}, the cumulative heat curve was fit nonlinearly based on Eq. (10). The remaining kinetic parameters (i.e., n, K_1', K_2', and K_3') could

be calculated through fitting according to Eqs. (1–3), respectively. Fig. 16 illustrates the determination of parameters of hydration kinetics of sample hydrated at w/c of 0.08. Other calculations of parameters of hydration kinetics of sample hydrated at w/c of 0.10−0.30 are presented in Figs. A1–A5.

$$A(t) = \frac{Q(t)}{Q_{max}} \tag{7}$$

$$\frac{d\alpha}{dt} = \frac{1}{Q_{max}} \cdot \frac{dQ}{dt} \tag{8}$$

$$\frac{1}{Q(t)} = \frac{1}{Q_{max}} + \frac{t_{50}}{Q_{max}(t - t_0)} \tag{9}$$

$$Q(t) = \frac{Q_{max}(t - t_0)}{(t - t_0) + t_{50}} \qquad (10)$$

where $\alpha(t)$ is degree of hydration; $Q(t)$ is the cumulative heat; Q_{max} is the theoretical maximum cumulative heat; $d\alpha/dt$ and dQ/dt represent the hydration rate; and t_{50} is the time when the cumulative heat reached 50% of Q_{max}.

3.2.2. Results of parameters of hydration kinetics

The hydration rate of PC could be calculated by substituting the parameters of hydration kinetics determined in section 3.2.2 into Eqs. (4), (5) and (6) and the results are presented in Fig. 17. It was obviously that the model was suitable to represent the hydration mechanism of PC hydrated at w/c ratios of 0.08−0.16 and of 0.30, and the PC hydration at w/c below 0.16 was not dominated by the I process. The hydration mechanisms and kinetic parameters of PC are summarized in Table 4. The exponent of geometrical crystal growth (n) improved with increase of w/c ratios from 0.08 to 0.16. Yet, the value of n reached up to 1.983 at w/c of 0.16, which was more than that of sample hydrated at w/c of 0.30. Hence, there was a significant influence of changing w/c on the exponent of geometrical crystal growth in hydration process of PC. The value of K_1' was apparently higher than K_2' and K_3' for PC hydratedat a determined w/c ratio, suggesting the hydration rate of NG process was much faster than that of I process and D process. Additionally, K_1', K_2' and K_3' reduced with raising w/c ratios, indicating that the hydration rate of PC decreased with raising w/c values. It could also be explained by increase in pH of pore solution with reducing w/c values [38]. In addition, the time when the cumulative heat reached up to 50 % of Q_{max} (i.e., t_{50}) increased with raising w/c values. It was consistent with Fig. 8 in which the time of the main heat evolution improved with raising w/c ratios. From Fig. 17, the hydration of PC at w/c ratios below 0.16 involved two processes: the NG process and D process, representing the hydration mechanism NG-D. The hydration reaction was dominated by the NG process in the early age, and D process played a significant role in the later hydration age. The hydration mechanism of PC at w/c of 0.30 was NG-I-D (Fig. 17 and Table 4), which was different from PC at w/c ratios below 0.16. This was probably due to chance that the pH might increase with decreasing w/c, and the hydration reaction of PC was accelerated by the higher pH.
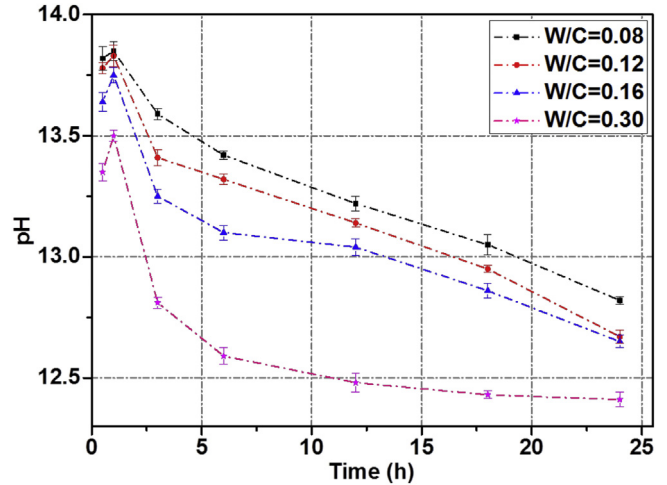

Fig. 18 – Alkalinity of pore solution of hardened pastes.

3.3. Alkalinity and concentrations of K^+ and Na^+ of pore solution

The alkalinity of pore solution of hydrated PC pastes is given in Fig. 18. Compared with the sample hydrated at w/c of 0.08, the alkalinities of pore solution of samples hydrated at w/c of 0.16 and 0.30 decreased by 0.18 and 0.47, respectively. Therefore, the alkalinity of pore solution decreased with increasing of w/c ratios. The phenomena could be explained by the alkali metal ions (i.e., K^+ and Na^+) of cement being mainly in the form of sulfate and solid solution, and the alkali metal ions in the form of sulfate dissolve rapidly when mixing cement and water. The concentrations of K^+ and Na^+ of pore solution decreased with raising w/c ratios (Fig. 19). After 1 h, the alkalinity of the pore solution decreased with increasing leaching time, especially for leaching times from 1 to 3 h. For instance, the alkalinities of pore solution of hardened pastes decreased to 13.59 and 12.81 at a leaching time of 3 h at w/c of 0.08 and 0.30, respectively. This could be attributed to the decrease of the concentration of K^+ and Na^+ of pore solution (Fig. 19), as the K^+ and Na^+ were absorbed by C-S-H gel [39]. There is a phenomenon worthy noting here, the alkalinities of samples at w/c of 0.08−0.16 were more than 13 when the leaching time was less than 12 h. However, the alkalinity of hardened paste was lower than 12.60 at w/c of 0.30 when the leaching time was more than 6 h. As
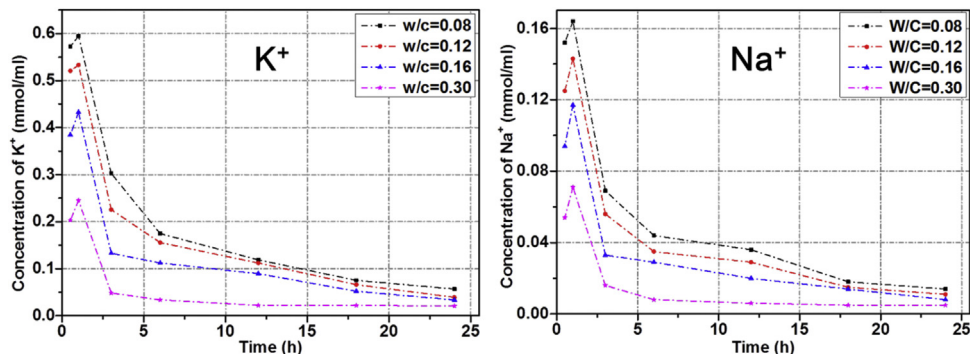

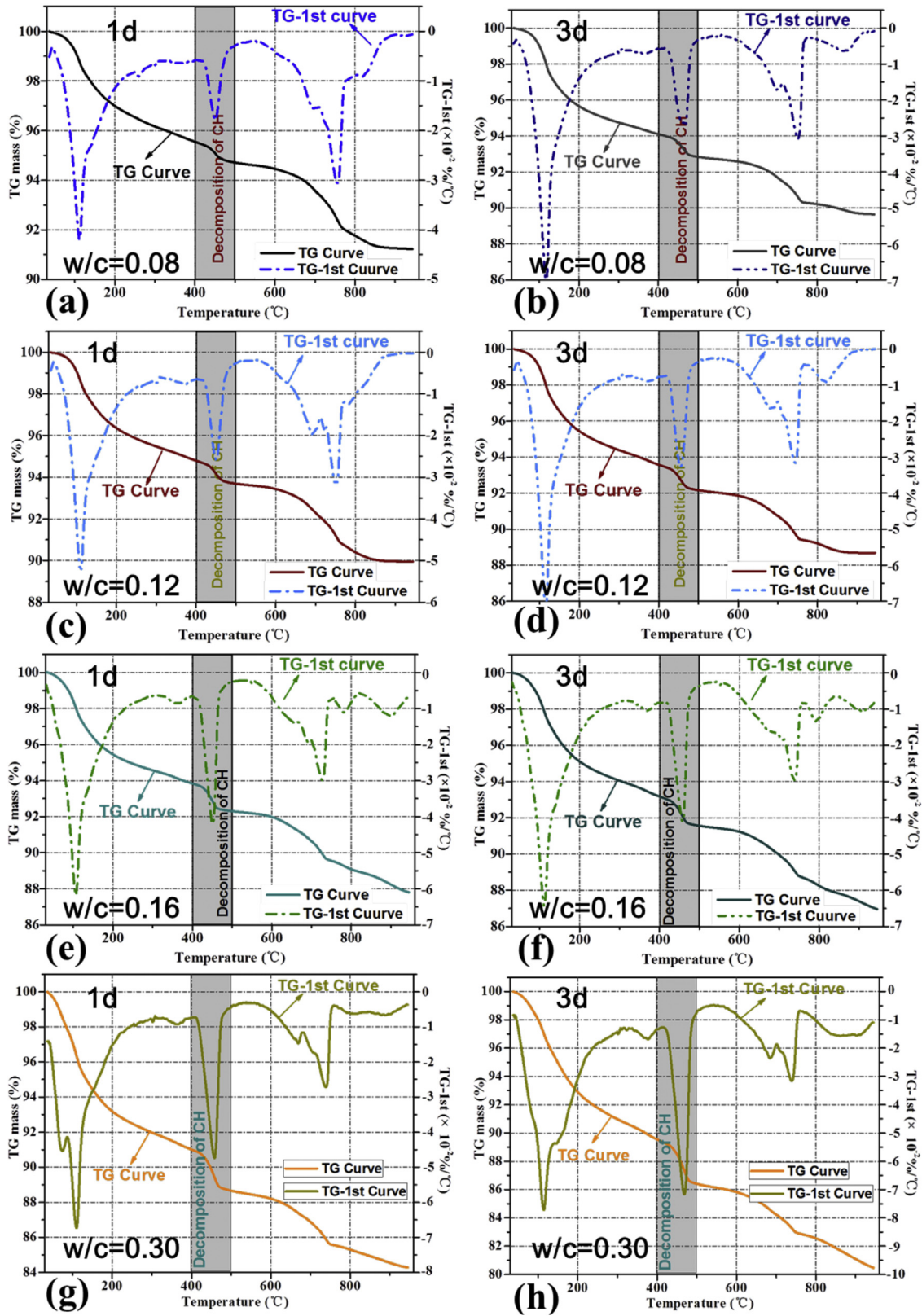Fig. 19 – Concentrations of K^+ and Na^+ of pore solution.

Fig. 20 – TG analysis: (a) w/c = 0.08, Hydration for 1 day; (b) w/c = 0.08, Hydration for 3 days; (c) w/c = 0.12, Hydration for 1 day; (d) w/c = 0.12, Hydration for 3 days; (e) w/c = 0.16, Hydration for 1 day; (f) w/c = 0.16, Hydration for 3 days; (g) w/c = 0.30, Hydration for 1 day; (h) w/c = 0.16, Hydration for 3 days.
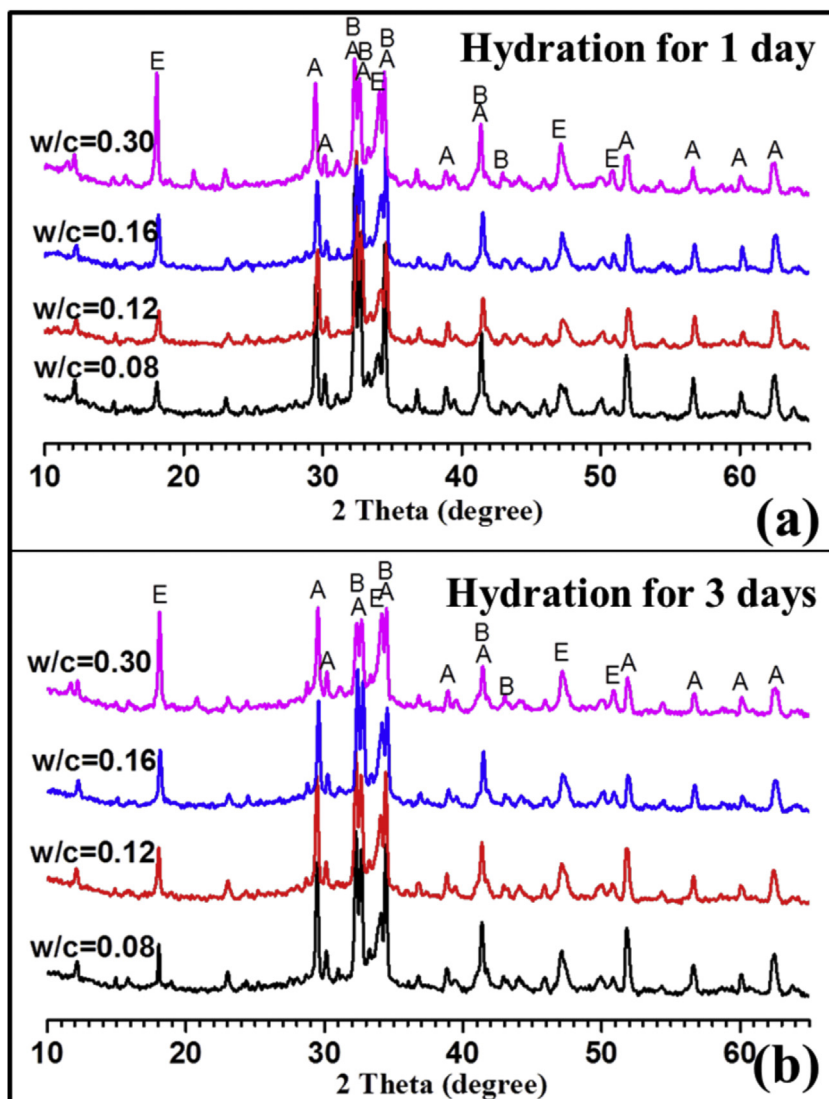
Fig. 21 – X-ray diffraction of hydration products (where A = Tricalcium silicate (C₃$), B = Dicalcium silicate (C₂$), E = calcium hydroxide (Ca(OH)₂).

is well known, the reaction rate of hydration increased with increasing alkalinity of the solution. Hence, it suggested that the HF_{max} of the paste with a w/c of 0.16 higher than that of paste with a w/c ratio of 0.30 (Fig. 13) and the changing of hydration mechanism (Table 4) could be attributed to the higher alkalinity of pore solution.
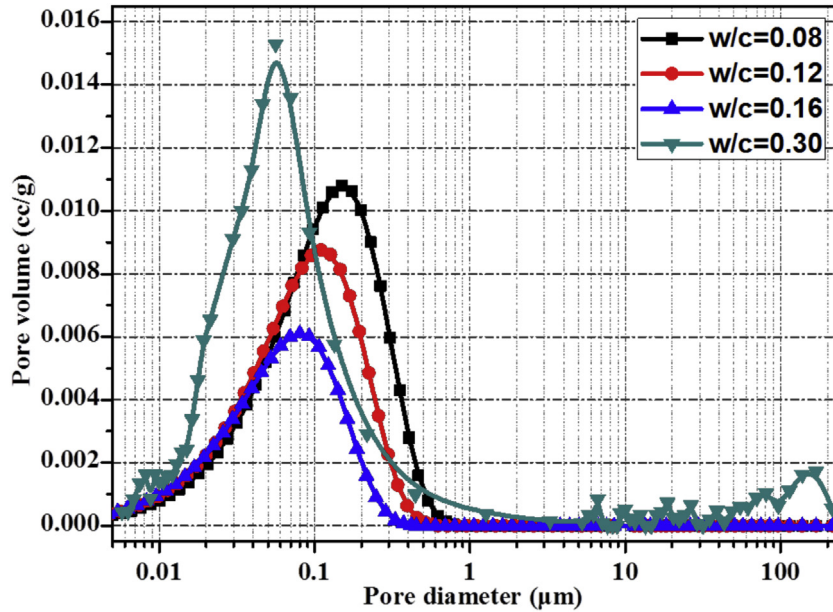
3.4. Analyses of hydration products

The data of TG analysis and X-ray diffraction are presented in Figs. 20 and 21. The total loss of mass of hydrated paste improved with raising w/c ratios (Fig. 20), and the crystalline mineral compositions were consistent with others (Fig. 21). Therefore, the degree of cement hydration improved with raising w/c values. Compared with w/c of 0.08, the 3-days total loss of mass of hydrated paste increased by 26.0 % to a value of 13.1 % at the w/c ratio of 0.16. This result was consistent with Fig. 13 in which the cumulative heat of hydration for 3 days improved
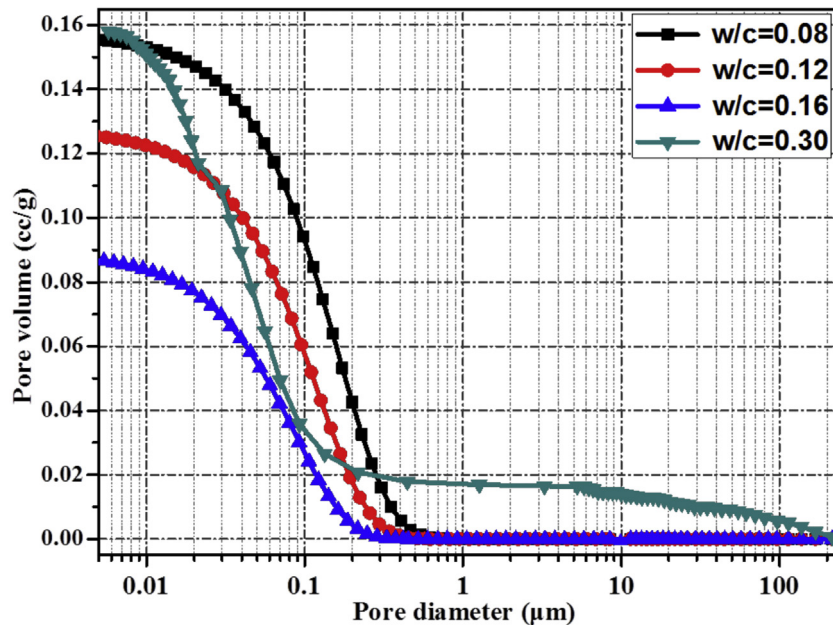
with raising w/c values. This might be because the space for hydration products growth (Fig. 9) and the amount of water available for the reaction improved by raising w/c values. In addition, the loss of mass of samples hydrated at w/c of below 0.16 increased with the increasing w/c values at 50–300 °C and 400–500 °C, which respectively represented C-S-H gel and CH decomposition [40,41]. The increasing of amount of hydration products was beneficial to reducing porosity and to increasing the fracture energy of hardened pastes.

3.5. Pore structure

Fig. 22 presents the pore structure of hydrated PC pastes cured for 3 days. In cases of w/c ratios below 0.16, the total pore volume decreased with raising w/c ratios (Fig. 22b). The total pore volume of hardened paste with w/c ratio of 0.16 decreased to 0.088 cc/g, a decrease of 43.6 % compared with that of sample with w/c ratio of 0.08. The decrease of pore

(a) Pore size distribution.
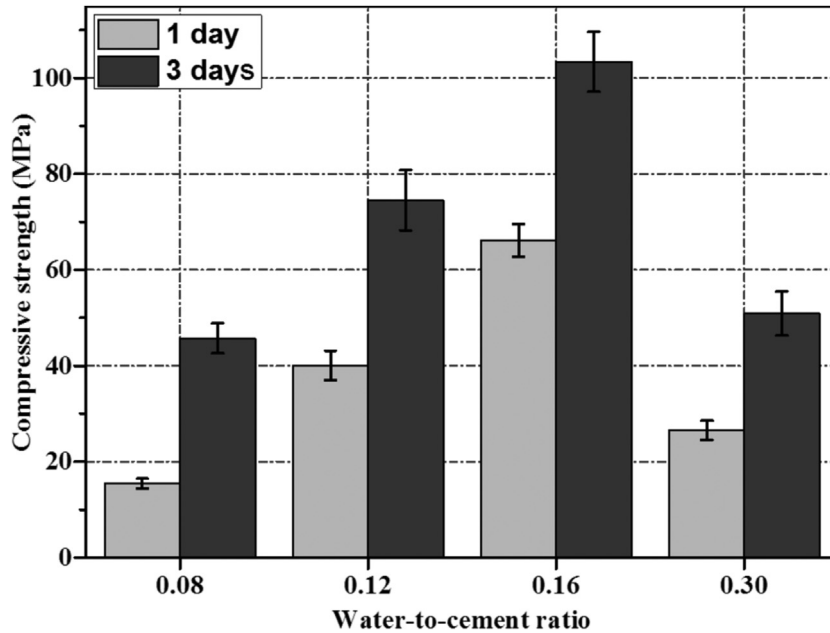

(b) Cumulative pore volume.

Fig. 22 – Pore structure of hardened pastes curing for 3 days.

volume could be attributed to the fine pores below $1\,\mu m$ in diameter (Fig. 22a). This phenomenon could be explained by the space available for hydration products growth (Fig. 9) and the amount of hydration products (Figs. 13 and 20) increased with raising w/c ratios while the w/c ratios blow 0.16. However, the total pore volume of sample hydrated at w/c of 0.30 reached to 0.158 cc/g, which was higher than that of sample hydrated at w/c of0.08. This was probably because of the space taken up by water not being totally filled by hydration

products and the bubbles (corresponding to the pores with diameters over $100\,\mu m$) being introduced into the paste when mixing.

3.6.   Mechanical properties

In cases of a w/c ratio of no more than 0.16, the compressive strength (Fig. 23a) and flexural strength (Fig. 23b) of hardened pastes improved with raising w/c ratios. The 3-days compres-
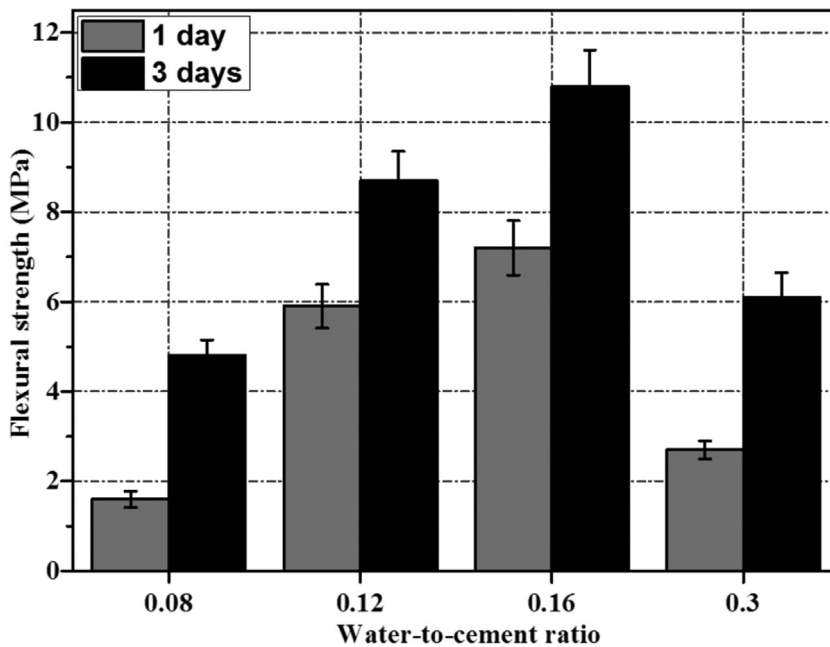
(a) Compressive strength.

Fig. 23 – Mechanical properties of hardened pastes.

sive strength and flexural strength of sample with w/c ratio of 0.16 increased by 126.3% and 125.0% to values of 103.4 MPa and 10.7 MPa compared with that of sample with w/c ratio of 0.08. The works of Balshin [42] and Ryshkewitch [43] on relationship of compressive strength and total pore volume of hydrated PC pastes suggested that there was an inversely proportional relationship between the two parameters. Therefore, this result identified with Fig. 22 in which the total pore volume of hardened paste reduced with raising w/c ratios.

When the w/c ratio increased to 0.30, the 3-day compressive strength was reduced to 48.9 MPa. This could be attributed to the improvement of the total pore volume (Fig. 22b). However, the 3-days flexural strength of sample hydrated at w/c of 0.30 was 6.1 MPa, apparently higher than that of sample hydrated at w/c of 0.08 although the total pore volume of both was almost the same. According to the study of Bocciarelli and Ranzi [44], the flexural strength of hardened paste was directly proportional to its fracture energy. Therefore, it might

be because the content of C-S-H gel of sample hydrated at w/c of 0.30 being higher than that of sample hydrated at w/c of 0.08 (Fig. 20), and the sample hydrated at w/c of 0.30 having a higher fracture energy.

4. Conclusions

Ice particles were adopted as mixing water to prepare the homogenous structural Portland cement (PC) pastes at super low w/c ratios from 0.08 to 0.16. The sample with a normal w/c ratio of 0.30 was prepared as reference. The early-age hydration characteristics and kinetics, mechanical properties, alkalinity and concentrations of K^+ and Na^+ of pore solution, hydration products and pore structure were investigated. The investigation supported the following conclusions:

1) With the increasing of w/c ratios, the acceleration period of hydration process of PC pastes prolonged due to that the space available for hydration products growth improved by increasing w/c ratios in acceleration period.
2) The maximum hydration reaction rate of cement changes under super low w/c ratio. In general, the maximum hydration reaction rate will increase with the increase of w/c ratio. However, the maximum hydration reaction rate was 34.51×10^{-4} mW/mg at w/c of 0.16, which was slightly higher than that of 34.12×10^{-4} mW/mg at w/c ratio of 0.30. It was mainly because the alkalinity of the pore solution with larger concentration of Na^+ and K^+ ions is higher when the w/c ratio is 0.16, which accelerated the hydration of cement.
3) The hydration mechanism of PC paste was 'NG-D' at w/c ratio of 0.08−0.16, which was different from the 'NG-I-D' hydration mechanism of the reference.
4) In cases of w/c ratios of less than 0.16, the compressive strength and flexural strength of hardened PC paste increased with increasing w/c ratios. It was mainly because of the porosity of hardened PC paste decreased with the increasing of w/c ratios in a range of 0.08 to 0.16.

The list of acronyms

No.	Acronym	Parameter description
1	w/c	Water-to-cement
2	PC	Portland cement
3	ICP-OES	Inductively Coupled Plasma Optical Emission Spectrometer
4	NG	Nucleation and crystal growth
5	I	Phase boundary reaction
6	D	Diffusion
7	UHPC	Ultra- high-performance concrete
8	RPC	Reactive powder concrete
9	PCC	Portland cement clink
10	XRD	X-ray diffraction
11	TG	Thermo-gravimetric

Conflicts of interest

The authors declare no conflict of interest.

Acknowledgments

Appendix A. Calculation of kinetics parameters of cement pastes with w/c ratios of 0.10, 0.12, 0.14, 0.16 and 0.30
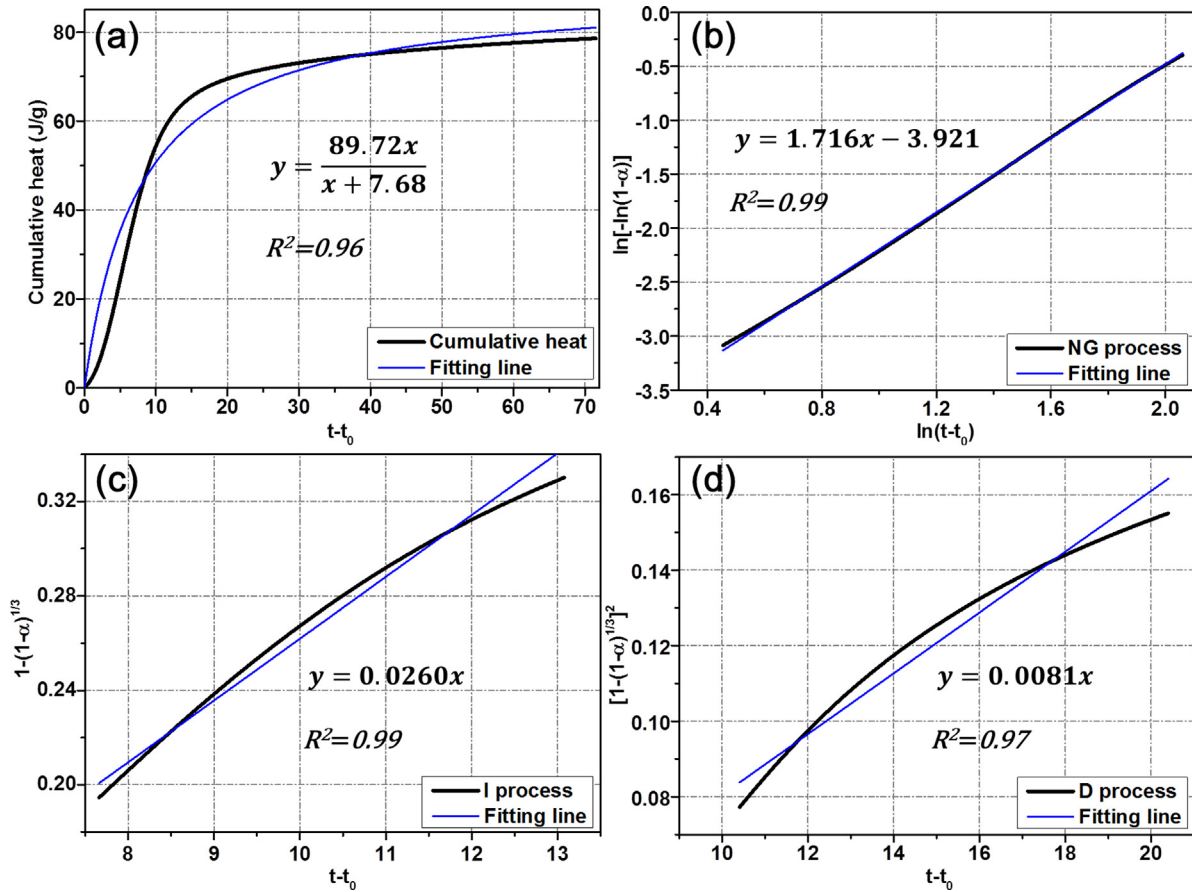
See Figs. A1–A5.

Fig. A1 – Calculation of kinetics parameters from the non-linear fitting and linear fitting at w/c ratio of 0.10; (a) Determination of Q_{max} and t_{50}, (b) Determination of n and K'_1, (c) Determination of K'_2, and (d) Determination of K'_3.

Fig. A2 – Calculation of kinetics parameters from the non-linear fitting and linear fitting at w/c ratio of 0.12; (a) Determination of Q_{max} and t_{50}, (b) Determination of n and K_1', (c) Determination of K_2', and (d) Determination of K_3'.
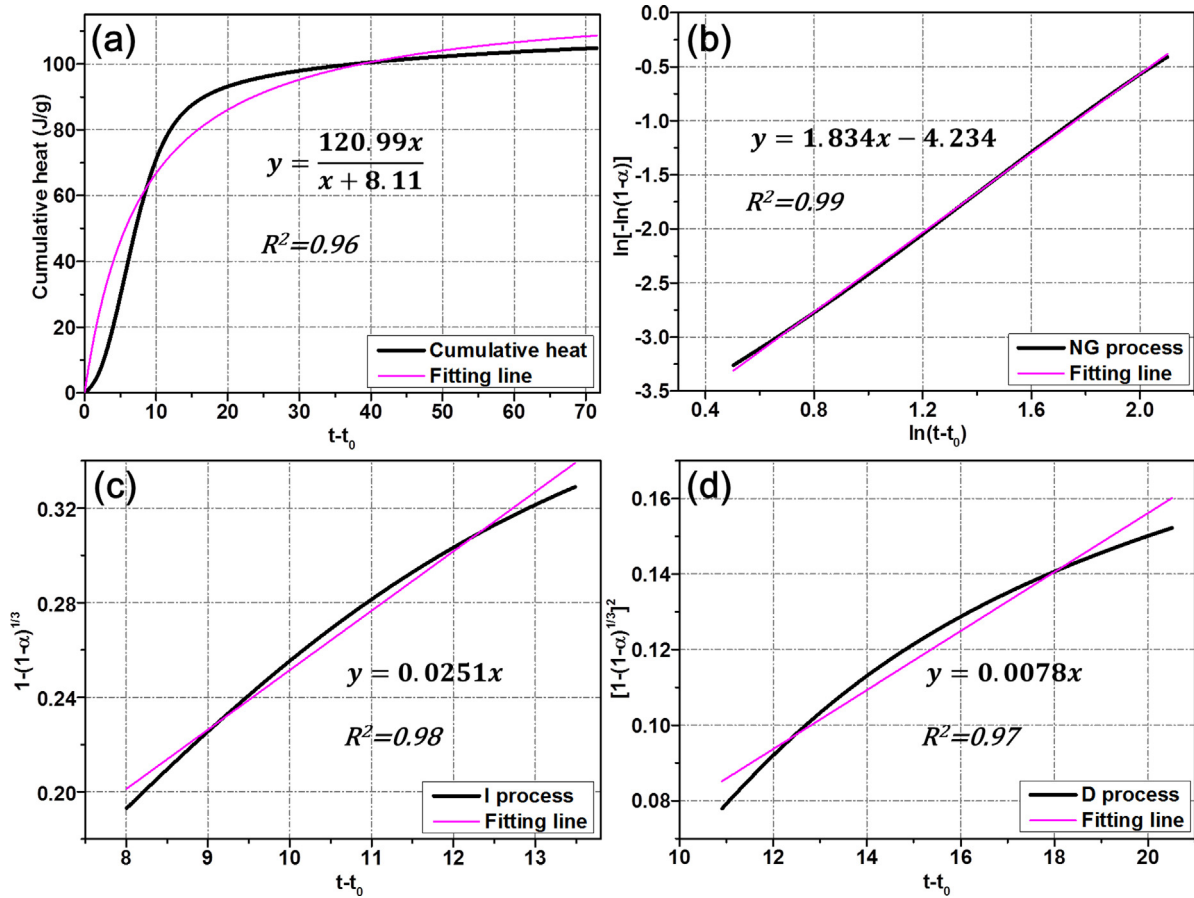
Fig. A3 – Calculation of kinetics parameters from the non-linear fitting and linear fitting at w/c ratio of 0.14; (a) Determination of Q_{max} and t_{50}, (b) Determination of n and K'_1, (c) Determination of K'_2, and (d) Determination of K'_3.
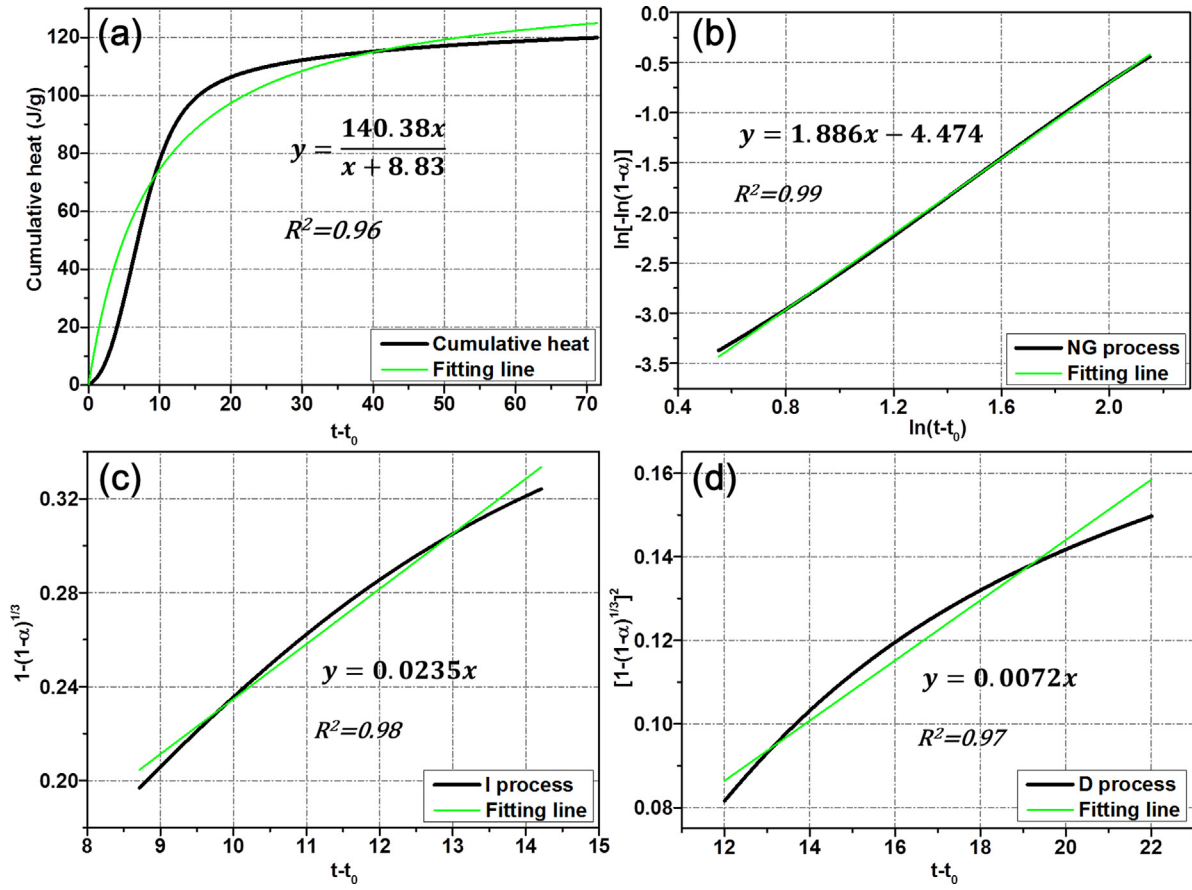
Fig. A4 – Calculation of kinetics parameters from the non-linear fitting and linear fitting at w/c ratio of 0.16; (a) Determination of Q_{max} and t_{50}, (b) Determination of n and K_1', (c) Determination of K_2', and (d) Determination of K_3'.
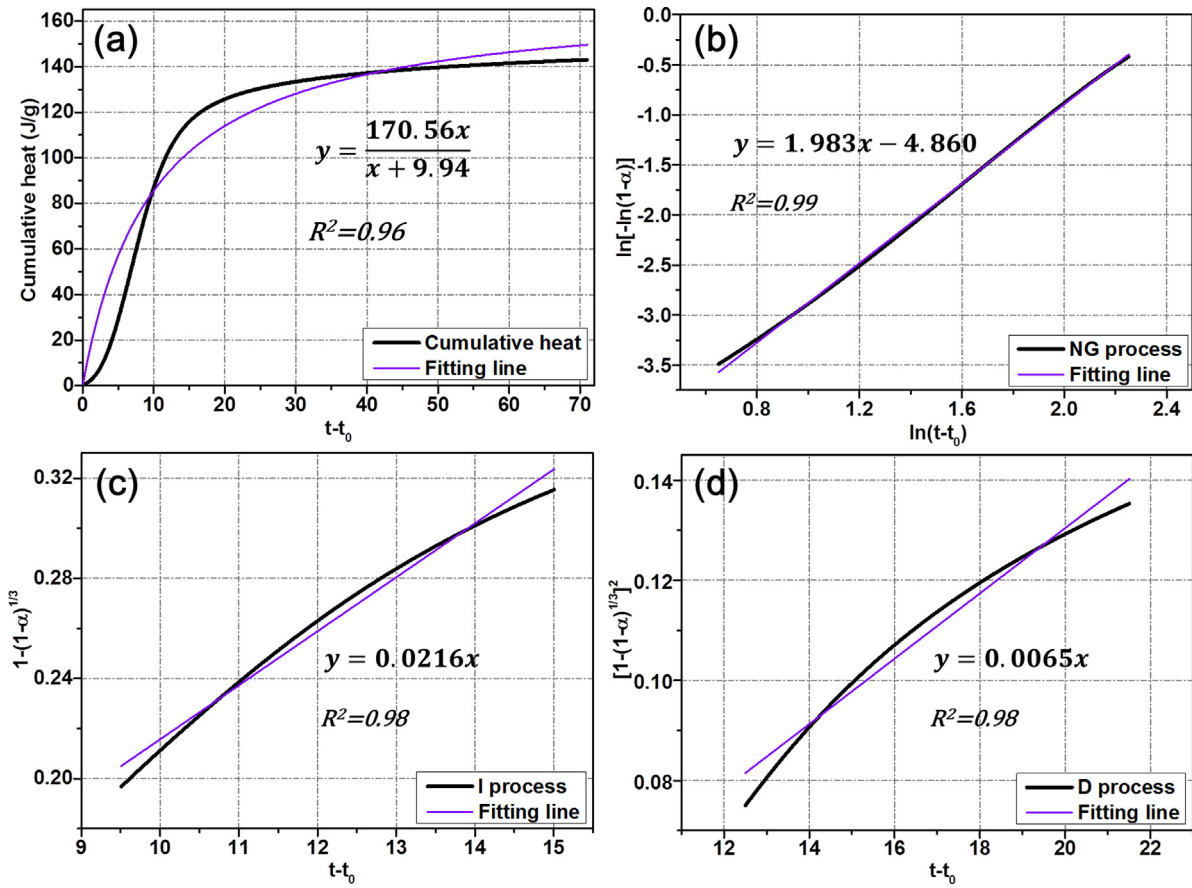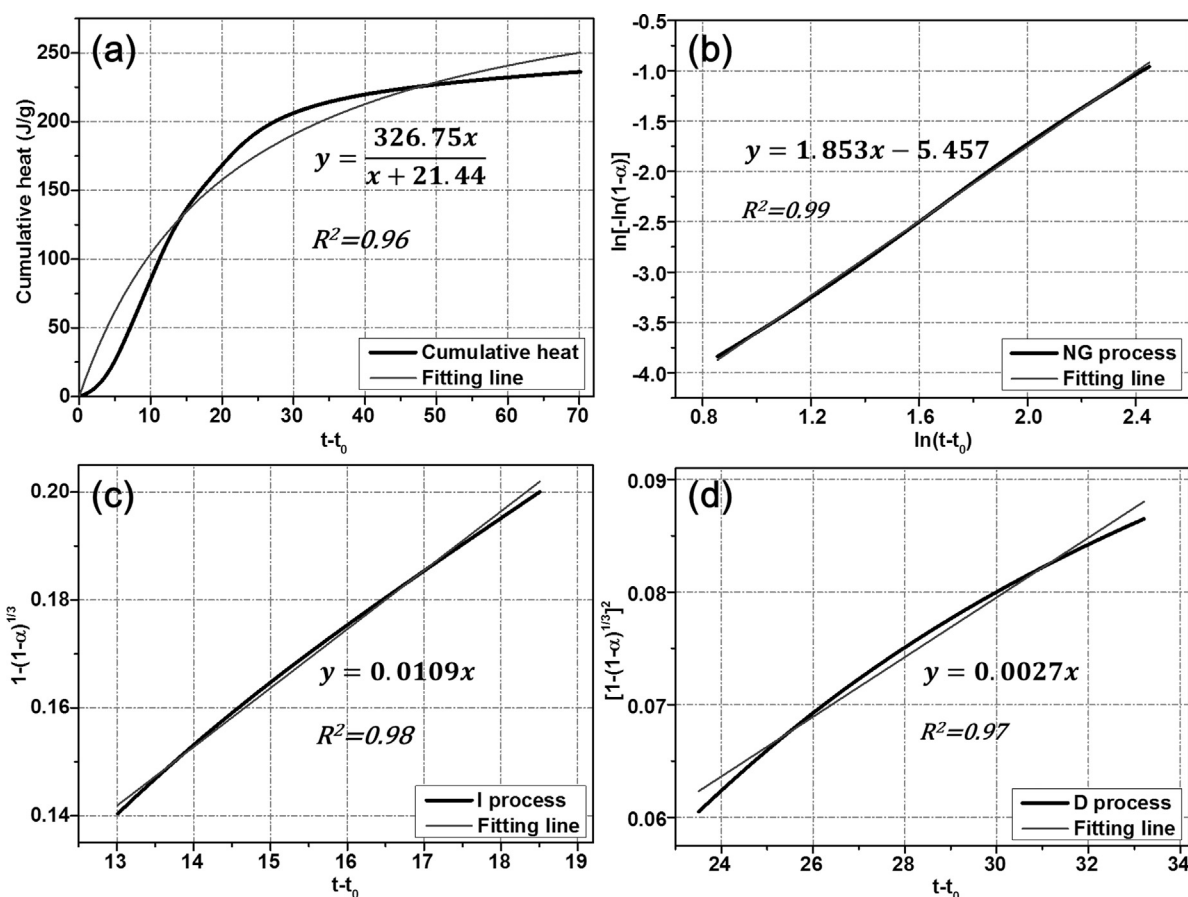
Fig. A5 – Calculation of kinetics parameters from the non-linear fitting and linear fitting at w/c ratio of 0.30; (a) Determination of Q_{max} and t_{50}, (b) Determination of n and K_1', (c) Determination of K_2', and (d) Determination of K_3'.

REFERENCES

[1] Marinković S, Dragaš J, Ignjatović I, Tošić N. Environmental assessment of green concretes for structural use. J Clean Prod 2017;154:633–49 https://doi.org/10.1016/j.jclepro.2017.04.015.

[2] DeRousseau MA, Kasprzyk JR, Srubar WV. Computational design optimization of concrete mixtures: a review. Cem Concr Res 2018;109:42–53, http://dx.doi.org/10.1016/j.cemconres.2018.04.007.

[3] Živica V. Effects of the very low water/cement ratio. Constr Build Mater 2009;23:3579–82, http://dx.doi.org/10.1016/j.conbuildmat.2009.03.014.

[4] Yudenfreund M, Hanna KM, Skalny J, Odler I, Brunauer S. Hardened Portland cement pastes of low porosity, V. Compressive strength. Cem Concr Res 1972;2:731–43, http://dx.doi.org/10.1016/0008-8846(72)90073-7.

[5] Bache HH. Densified cement/ultra-fine particle-based materials. In: Proc. International Conference on Superplasticizers in Concrete. 1981. p. 12.

[6] Cwirzen A, Penttala V, Vornanen C. Reactive powder based concretes: mechanical properties, durability and hybrid use with OPC. Cem Concr Res 2008;38:1217–26, http://dx.doi.org/10.1016/j.cemconres.2008.03.013.

[7] Abid M, Hou X, Zheng W, Hussain RR. High temperature and residual properties of reactive powder concrete - A review. Constr Build Mater 2017;147:339–51, http://dx.doi.org/10.1016/j.conbuildmat.2017.04.083.

[8] Yoo DY, Banthia N, Kim SW, Yoon YS. Response of ultra-high-performance fiber-reinforced concrete beams with continuous steel reinforcement subjected to low-velocity impact loading. Compos Struct 2015;126:233–45, http://dx.doi.org/10.1016/j.compstruct.2015.02.058.

[9] Nguyen DL, Kim DJ, Ryu GS, Koh KT. Size effect on flexural behavior of ultra-high-performance hybrid fiber-reinforced concrete. Compos Part B-Eng 2013;45(1):1104–16, http://dx.doi.org/10.1016/j.compositesb.2012.07.012.

[10] Rossi P, Arca A, Parant E, Fakhri P. Bending and compressive behaviours of a new cement composite. Cem Concr Res 2005;35(1):27–33, http://dx.doi.org/10.1016/j.cemconres.2004.05.043.

[11] Zhou M, Lu W, Song J, Lee GC. Application of ultra-high performance concrete in bridge engineering. Constr Build Mater 2018;186:1256–67, http://dx.doi.org/10.1016/j.conbuildmat.2018.08.036.

[12] Kang SH, Hong SG, Moon J. The use of rice husk ash as reactive filler in ultra-high performance concrete. Cem Concr Res 2019;115:389–400, http://dx.doi.org/10.1016/j.cemconres.2018.09.004.

[13] Shi Y, Long G, Ma C, Xie Y, He J. Design and preparation of ultra-high performance concrete with low environmental impact. J Clean Prod 2019;214:633–43, http://dx.doi.org/10.1016/j.jclepro.2018.12.318.

[14] Pedro D, Brito de J, Evangelista L. Mechanical characterization of high performance concrete prepared with recycled aggregates and silica fume from precast

industry. J Clean Prod 2017;164:939–49,
http://dx.doi.org/10.1016/j.jclepro.2017.06.249.

[15] Pourbaba M, Joghataie A, Mirmiran A. Shear behavior of ultra-high performance concrete. Constr Build Mater 2018;183:554–64,
http://dx.doi.org/10.1016/j.conbuildmat.2018.06.117.

[16] Li W, Fall M. Sulphate effect on the early age strength and self-desiccationof cemented paste backfill. Constr Build Mater 2016;106:296–304,
http://dx.doi.org/10.1016/j.conbuildmat.2015.12.124.

[17] Arend J, Wetzel A, Middendorf B. In-situ investigation of superplasticizers: from fluorescence microscopy to concrete rheology. Cem Concr Res 2018;113:178–85,
http://dx.doi.org/10.1016/j.cemconres.2018.08.011.

[18] Damme van H. Concrete material science: past, present, and future innovations. Cem Concr Res 2018;112:5–24,
http://dx.doi.org/10.1016/j.cemconres.2018.05.002.

[19] Ekincioglu O, Ozkul MH, Struble LJ, Patachia S. Optimization of material characteristics of macro-defect free cement. Cem Concr Comp 2012;34:556–65,
http://dx.doi.org/10.1016/j.cemconcomp.2011.11.003.

[20] Shen Y, Deng M, Lu A. Structural evolution of hydrated cement compacts. Mater Struct 2011;44:1735–43,
http://dx.doi.org/10.1617/s11527-011-9731-z.

[21] Lecomte A, Mechling JM, Diliberto C. Compaction index of cement paste of normal consistency. Constr Build Mater 2009;23(10):3279–86,
http://dx.doi.org/10.1016/j.conbuildmat.2009.05.005.

[22] GB (2007) GB 175-2007: Common Portland cement. Standarization Administration of the People's Republic of China, Beijing, China. (in Chinese, equivalent to ENV 197-1: Common Portland cement. European Committee for Standardization, 2000.

[23] Thomas JJ. A new approach to modeling the nucleation and growth kinetics of tricalcium silicate hydration. J Am Ceram Soc 2007;90(10):3282–8,
http://dx.doi.org/10.1111/j.1551-2916.2007.01858.x.

[24] Cheung J, Jeknavorian A, Roberts L, Silva D. Impact of admixtures on the hydration kinetics of Portland cement. Cem Concr Res 2011;41(12):1289–309,
http://dx.doi.org/10.1016/j.cemconres.2011.03.005.

[25] Wang T, Xue Y, Zhou M, Lv Y, Chen Y, Wu S, et al. Hydration kinetics, freeze-thaw resistance, leaching behavior of blended cement containing co-combustion ash of sewage sludge and rice husk. Constr Build Mater 2017;131:361–70,
http://dx.doi.org/10.1016/j.conbuildmat.2016.11.087.

[26] Han F, Zhang Z, Wang D, Yan P. Hydration heat evolution and kinetics of blended cement containing steel slag at different temperatures. Thermochim Acta 2015;605:43–51,
http://dx.doi.org/10.1016/j.tca.2015.02.018.

[27] Zhu B, Song Y, Li X, Chen P, Ma Z. Synthesis and hydration kinetics of calcium aluminate cement with micro $MgAl_2O_4$ spinels. Mater Chem Phys 2015;154:158–63,
http://dx.doi.org/10.1016/j.matchemphys.2015.01.060.

[28] Thomas JJ, Biernacki JJ, Bullard JW, Bishnoi S, Dolado JS, Scherer GW, et al. Modeling and simulation of cement hydration kinetics and microstructure development. Cem Concr Res 2011;41:1257–78,
http://dx.doi.org/10.1016/j.cemconres.2010.10.004.

[29] Liu L, Yang P, Qi C, Zhang B, Guo L, Song KI. An experimental study on the early-age hydration kinetics of cemented paste backfill. Constr Build Mater 2019;212:283–94,
http://dx.doi.org/10.1016/j.conbuildmat.2019.03.322.

[30] Zuo Y, Nedeljković M, Ye G. Pore solution composition of alkali-activated slag/fly ash pastes. Cem Concr Res 2019;115:230–50,
http://dx.doi.org/10.1016/j.cemconres.2018.10.010.

[31] Scrivener KL, Juilland P, Monteiro PJM. Advances in understanding hydration of Portland cement. Cem Concr Res 2015;78:38–56,
http://dx.doi.org/10.1016/j.cemconres.2015.05.025.

[32] Bishnoi S, Scrivener KL. Studying nucleation and growth kinetics of alite hydration using μic. Cem Concr Res 2009;39:849–60,
http://dx.doi.org/10.1016/j.cemconres.2009.07.004.

[33] Bazzoni A, Ma S, Wang Q, Shen X, Cantoni M, Scrivener KL. The effect of magnesium and zinc ions on the hydration kinetics of C_3S. J Am Ceram Soc 2014;97:3684–93,
http://dx.doi.org/10.1111/jace.13156.

[34] Coumes CCD Courtois S, Nectoux D, Leclercq S, Bourbon X. Formulating a low-alkalinity, high-resistance and low-heat concrete for radioactive waste repositories. Cem Concr Res 2006;36(12):2152–63,
http://dx.doi.org/10.1016/j.cemconres.2006.10.005.

[35] Bullard JW, Jennings HM, Livingston RA, Nonat A, Scherer GW, Schweitzer JS, et al. Mechanisms of cement hydration. Cem Concr Res 2011;41:1208–23,
http://dx.doi.org/10.1016/j.cemconres.2010.09.011.

[36] Minard H, Garrault S, Regnaud L, Nonat A. Mechanisms and parameters controlling the tricalcium aluminate reactivity in the presence of gypsum. Cem Concr Res 2007;37:1418–26,
http://dx.doi.org/10.1016/j.cemconres.2007.06.001.

[37] Bazzoni A. Study of early hydration mechanisms of cement by means of electron microscopy. Thèse EPFL n°6296 2014
http://infoscience.epfl.ch/record/200217/files/EPFL_TH6296.pdf).

[38] Juenger MCG, Siddique R. Recent advances in understanding the role of supplementary cementitious materials in concrete. Cem Concr Res 2015;71–80,
http://dx.doi.org/10.1016/j.cemconres.2015.03.018.

[39] Brouwers HJH, Eijk RJV. Alkali concentrations of pore solution in hydrating OPC. Cem Concr Res 2003;33:191–6,
http://dx.doi.org/10.1016/S0008-8846(02)01022-0.

[40] Li L, Zhou X, Li Y, Gong C, Lu L, Fu X, et al. Water absorption and water/fertilizer retention performance of vermiculite modified sulphoaluminate cementitious materials. Constr Build Mater 2017;137:224–33,
http://dx.doi.org/10.1016/j.conbuildmat.2017.01.061.

[41] Lu Z, Hou D, Ma H, Fan T, Li Z. Effects of graphene oxide on the properties and microstructures of the magnesium potassium phosphate cement paste. Constr Build Mater 2016;119:107–12,
http://dx.doi.org/10.1016/j.conbuildmat.2016.05.060.

[42] Pandey SP, Sharma RL. The influence of mineral additive on strength and porosity of OPC mortar. Cem Concr Res 2000;30:19–23,
http://dx.doi.org/10.1016/S0008-8846(99)00180-5.

[43] Kearsley EP, Wainwright PJ. The effect of porosity on the strength of foamed concrete. Cem Concr Res 2002;32:233–9,
http://dx.doi.org/10.1016/S0008-8846(01)00665-2.

[44] Bocciarelli M, Ranzi G. Identification of the hygro-thermo-chemical-mechanical model parameters of concrete through inverse analysis. Constr Build Mater 2018;162:202–14,
http://dx.doi.org/10.1016/j.conbuildmat.2017.11.167.

[45] Li L, Zhang H, Guo X. Pore structure evolution and strength development of hardened cement paste with super low water-to-cement ratios. Constr Build Mater 2019;227:117108,
http://dx.doi.org/10.1016/j.conbuildmat.2019.117108.